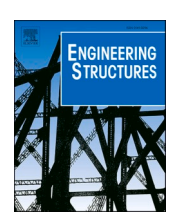
ELSEVIER

Contents lists available at ScienceDirect

Engineering Structures

journal homepage: www.elsevier.com/locate/engstruct





Finite element analysis of low-rise non-engineered timber residential buildings in Dominica under hurricane loads

Sarah Esper ^a, Dina D'Ayala ^{a,b,*}

- ^a EPICentre, Department of Civil, Environmental and Geomatic Engineering, University College London, London, United Kingdom
- b UNESCO Chair in Disaster Risk Reduction and Resilience Engineering, Department of Civil Environmental and Geomatic Engineering, University College London, London, United Kingdom

ARTICLE INFO

Keywords:
Residential buildings
Caribbean
Wind loads
Timber building modelling
Hurricane loads

ABSTRACT

This study identifies the most common residential building typologies in Dominica, to analyse their structural response to hurricane loading. A detailed field survey was developed to undertake structural inspections of over 60 Dominica's low-rise, non-engineered residential buildings. The data was examined to build a representative prototype model of a typical timber residential building typology of high wind fragility. This typology refers to existing elevated timber buildings with lightweight hip roofs. An iterative process is developed to build the prototype model to analyse its structural response to wind loading applied in a quasi-static manner and calculated according to equations in ASCE 7–22. The numerical analysis is undertaken using the commercial software SAP2000. With connection details, frame element sizes and spacing for the prototype building falling short of existing building guidelines, the frame elements' nailed connections are expected to experience pull-out or slip failure before the building envelope is breached. The wind loading is directed toward the front of the building. It considers both positive and negative internal pressure, with the former leading to failure for lower wind speed. The inclusion of bracing elements at building corners reduces elastic lateral displacements; however, it also slightly reduces the wind speed at which the onset of failure occurs. A sensitivity analysis explores the stiffening effect of roof and wall sheathing, by varying the translational constraints at the building corners, which is shown to affect the speed at which failure is initiated and the failure mode.

1. Introduction

Hurricanes affect numerous Caribbean states more frequently than other natural perils on an annual basis, negatively impacting their economies, due to the regional pattern of storm tracks and their increased frequency due to climate change; the orientation and shape of the islands, and the buildings' vulnerability to strong winds [46]. Non-engineered self-built homes are most exposed, while the limited structural information available hinders accurate analytical vulnerability assessment, which shall inform strengthening strategies, to be implemented at scale.

Despite recurring severe damage to timber houses caused by hurricanes across the Latin American and Caribbean (LAC) region, the insurance industry appears reluctant to provide cover [37], meaning that claim/damage data is limited for these structures. Therefore, empirical fragility assessment is difficult to pursue. Moreover, residential buildings being usually self-built with modest technical input, their response

is unlikely to conform to engineered models included in building codes.

He et al. [27] define four categories of studies on the performance of low-rise timber structures exposed to hurricanes: (1) vulnerability-based catastrophe models predicting economic loss; (2) deterministic finite element analysis of components and whole buildings; (3) component-level probabilistic building performance assessment; and (4) building tests in wind tunnels or under natural wind. Of particular relevance to this study are wind vulnerability assessment models and numerical modelling methodologies developed at the whole building level, relevant to Caribbean typologies.

Vulnerability studies are classified as empirical, e.g., Chock [13]; engineering-based, e.g., the Florida Public Hurricane Loss Model (FPHLM) [44]; and heuristic, e.g., CAPRA [11]. Methodologies relevant to the LAC region belong to the heuristic category. López and Godoy [36] applied the component-based ASCE 7–02 [4] methodology to determine the damage sequence of building components as a function of various wind speed intensity measures for metal industrial buildings in

^{*} Correspondence to: University College London, Gower Street, London, WC1E 6BT, UK. E-mail addresses: sarah.esper.12@ucl.ac.uk (S. Esper), d.ayala@ucl.ac.uk (D. D'Ayala).

Puerto Rico. Garcia Palencia et al. [23] studied progressive failure of envelop components and collapse inducing failure of column-foundation connections, to compute building level fragility functions.

Due to the lack of exposure data for building typologies in the Caribbean, Bertinelli et al. [7] resorted to satellite-derived nightlight intensity images as a proxy of local income, to determine the economic impact of tropical storms on a large number of Caribbean islands. The study uses a synthetic set of 4000 hurricane-strength storms and the general damage index derived by Emanuel [19] to represent the fraction of building damage at given wind speed. Using the same typology characterisation approach, Sealy and Strobl [50] determined threshold values of wind speed for 0 % and 50 % damage ratio for concrete block masonry buildings, designed according to the Bahamas Building Code [25].

Using expert judgement, CAPRA (Central America Probabilistic Risk Assessment initiative) is a modular hazard and risk assessment simulation platform comprising a hurricane predefined vulnerability model [11], fit to several countries. Using this approach, Yamin et al. [60], developed comprehensive wind vulnerability functions within the framework of the probabilistic global risk assessment undertaken as part of the UNISDR's Global Assessment Report on Disaster Risk Reduction, GAR13 [14]. The customisation of generic vulnerability functions to a specific country, is associated to a design level, this in turn dependent on specific criteria set for the building class and height, the development level of a country, the complexity level of a town/city, and the regional hazard level. Recent work by Valdivieso et al. [59] has used a component-based approach to define fragility functions for gable and hip truss roofs for 1 storey shear walls timber building in Puerto Rico, to determine annual probabilities of failure.

Regarding numerical modelling, He et al. [27] note the usefulness of fragility/vulnerability curves accounting for the critical structural responses quantifying building performance. The researchers recommend a stochastic finite element method to extend the classic deterministic approach.

Finite element method-based studies typically employ linear analysis using commercial software [32,38,39,43,62,63]. Asiz et al. [6] carried out a non-linear analysis in SAP2000. Pan et al. [41] used non-linear analysis in ANSYS [3] also in later related studies [30,29,28] as well as [22]. Modelling of connections varies in the above cases, being simulated as pinned or rigid, by releasing internal degrees of freedom, or introducing linear or non-linear springs at elements' joint. Most studies, however, borrow constitutive load-displacement curves for wood members and joints from literature, instead of using bespoke experimental data [16,48].

The wind loading sources for these studies are either obtained from measurements of wind tunnel pressures, computed according to building codes (most commonly ASCE 7 Standard) or derived from field measurements [62,63]. The latter performed numerical analysis for several load scenarios including field-acquired wind pressure time histories measured on a full-scale building. Static wind loading is used by [32,38,39,41,43,62,22].

Complete 3D numerical models aimed at determining highresolution results raise several challenges [27]. These involve convergence issues in the non-linear phase due to model complexity, often reducing to the linear range. Additionally, rarely they extend to collapse. Trautner and Ojdrovic [55] investigated effect of building configuration including bracing schemes on structural response, to identify different failure modes and sequences. Pan et al. [41] quantify the wind speeds causing first breach related to seven building envelope's failure modes under mean wind tunnel pressures. Fusco et al. [22] include failure of framing elements, besides sheathing failure, in their analysis, however, this is limited to the buckling of truss or rafter members.

The majority of the studies referenced above built numerical models for engineered, non-elevated timber framed buildings with gable roofs, typical of construction in North America. The transferability of these studies' findings to the global south is limited, due to differing structural typologies and construction practices and materials. Elevated buildings have not been an object of study, so far, except for [49], investigating probabilistic wind uplift resistance using a component to system approach, and [1,17,61] where the influence of elevating the structure on hurricane-induced flood and surge vulnerability was the main concern; however, considerations on wind vulnerability such as the building envelope connection to the timber floor deck is not considered. None of these typologies match the one considered in the present study.

This paper presents a finite element methodology for the analytical wind vulnerability assessment of low-rise, non-engineered elevated timber buildings with lightweight hip roofs. The objectives include: (1) visualising the failure modes of elevated building exposed to hurricane level wind loads, (2) incorporating three-dimensional system effects, due to asymmetric plan and the hip roof frame assembly, (3) accounting for as-built construction details for the building typology of interest as observed in the field. Due to their substantial redundancies, timber structures can sustain load past the initiation of damage of their most vulnerable component [41]. Therefore, this study investigates the sequence of failure leading to large displacements up to loss of lateral capacity, to determine damage prediction and mitigation strategies.

The proposed methodology fills a gap in current knowledge regarding construction methods and structural performance of typical Caribbean non-engineered residential building typologies, exposed to hurricane loads. Three other common Dominican residential building typologies were considered in this project, i.e. timber and concrete masonry buildings with light hip/hip & valley roofs, and concrete masonry buildings with either light hip/hip & valley roofs or with heavy flat roofs. Here we report on the elevated timber light hip roof typology because, while a less common typology in Dominica, it is the most vulnerable. Moreover, its construction is similar to the upper storey of timber and concrete block masonry buildings, a widespread typology across the whole Caribbean, with a correlated level of vulnerability.

2. Method

Given the non-engineered nature of the structures object of this study, the methodology (Fig. 1) draws on diverse sources of information to identify existing construction practices and building typologies, to reliably underpin a tool for wind vulnerability assessment applicable to the region of interest.

To produce a realistic numerical model, measurable quantities, including sizing and spacing of structural and non-structural elements and connections, as well as their material properties, are required. Some of these parameters are found in fragility and vulnerability literature as identifiers of building typologies. Therefore, the first stage of this methodology is concerned with the correlation of parameters used for typology identification and parameters essential to the numerical modelling. The second stage makes use of available empirical damage data, to identify vulnerable typologies and validate the analytical model. This requires construction, damage, and/or claim data for the residential typologies of interest. For Dominica, a island-wide building damage assessment was led by the United Nations Development Programme (UNDP) after Hurricane Maria (2017). Availability of the event wind speed geolocated estimates, allows performing an empirical fragility assessment providing insight on the relative performance of the exposed typologies.

Primary data collection is at the core of this methodology and takes place in the third stage. The data obtained in the second stage is compared with the required parameters identified in the first stage, to design and undertake a structural survey, targeting any outstanding information. From the statistical distribution of typologies identified in stage 2, a representative sample size is obtained for the fieldwork. Compliance of the as-built construction with existing codes/standards is examined. These field data is used to build a prototype numerical model for the typology of interest. In the present study the structural response to hurricane loads is assessed with a wind loading pressure distribution

Numerical Assessment Field Survey Parameter Selection Damage Data Analysis Identify construction Identify the common Design and undertake a Quantify the capacity of the parameters commonly residential building structural survey targeting existing structural and nonconsidered across fragility typologies existing across the outstanding construction structural connections. and vulnerability functions the region of interest. data for the typologies of for wind hazard. interest considering a Build a prototype numerical Obtain an empirical representative sample size. model for the typology of Identify construction fragility ranking of interest based on parameters required for the typologies by linking Compare the collected information collected in the numerical modelling of a damage to wind speed using structural data against field. existing housing guidelines. prototype building against available wind field wind loading. model(s). building codes, and Assess the structural standards. response of the building to Compare available hurricane wind loading construction data from the applied in an incrementally damage assessment with the increasing manner and required parameters. computed according to ASCE 7-22 MWFRS Case

Fig. 1. Methodology flowchart.

calculated according to ASCE 7–22 [5] Main Wind Force Resisting System (MWFRS) Case 1, accounting for elevated buildings. The loading is applied incrementally to allow for failure checks against the capacities of the structural connections and components.

2.1. Parameter selection for the numerical model

A thorough review of wind fragility and vulnerability functions published in the last two decades produced a first screening of the construction parameters used to differentiate building typologies. These are summarised in Table 1 for the structural components and in Table 2 for their connections. Most relevant construction parameters relate either to the roof construction, determining uplift failure, or of walls, resisting alternatively lateral pressure and suction. Floor and foundation construction is less detailed or overlooked.

A full 3D numerical model requires building plan and elevation dimensions, followed by specific details of the structural elements. The same logic is applied when collecting structural survey data on-site, including details for the roof, walls, floors, and foundations. Moreover, material details such as wood species, age, and quality should be known, as they influence structural performance and fragility/vulnerability.

The detailed structural survey, essential in the absence of as-built construction drawings, (further elaborated in Section 2.3) is designed to maximise the construction information and measurements collected in the field, both externally and internally, although acknowledging the limits imposed by the continued occupancy. Nonetheless, construction details hidden by finishings, including connections, roof cover, sheathing and below-ground foundation details, may require considering alternative sources, as suggested in Table 1 and Table 2. These sources are listed in order of preference and reliability. If (i) the field survey cannot reveal the required data, (ii) knowledge should be sought by local surveyors or, alternatively (iii) by engineers with local professional knowledge. The final option (iv) is to assume these details according to recommendations in local guidelines.

Table 1 and Table 2 summarise the value ranges of these construction parameters as surveyed in the field and provide the value adopted for the prototype model and its justification. Sections 2.3 and 2.4 elaborate further on the collection and use of the field data to build a representative single-storey prototype building. The availability of secondary data, such as the damage assessment discussed in Section 2.2, can be useful in determining the scope of primary data required to complement

the building information.

2.2. Damage data analysis

An island-wide building damage assessment was completed by the UNDP in Dominica within several months of the landfall of Hurricane Maria in September 2017. Information including the building use, exterior wall material, roof type, and number of storeys was collected for 29,431 geo-referenced buildings. Residential buildings were the focus of the building damage assessment by UNDP [56], and as such the 25,477 houses surveyed are expected to constitute most of Dominica's housing portfolio.

The UNDP data was examined to determine the population of single-storey timber buildings with galvanised sheeting hip/hip & valley/cross-hipped roofs (Typology TGH) and locate and survey a representative sample. Although this typology constitutes a modest proportion of the island's housing population, it is also one of the most vulnerable. Moreover, as an elevated building, its construction represents the second storey of the timber and concrete masonry buildings with galvanised sheeting hip/hip & valley/cross-hipped roofs, a common typology in Dominica.

Typology TGH is of interest, owing to the range of construction details contributing to structure's fragility, e.g., connections, member sizes and spacing, which are straightforward to retrofit, compared to other typologies. Addition of members or hurricane straps in the roof are implementable with modest disruption. Hip roofs perform better than gable roofs [20,54], as also demonstrated by the UNDP damage assessment statistics, however they are not commonly modelled in literature. Therefore, the structural response of this typology should prove immediately helpful to residents and professionals in Dominica, engaging in initiatives to rebuild better, such as the Dominica Housing Recovery Project (DHRP) [26].

A total of 262 houses were identified as TGH typology whose damage was due to Hurricane Maria (2017) windspeeds. The damage states adopted by this study according to the building tag colour assigned for the whole building by UNDP [56,57] are summarised in Table 3. However, the UNDP further recorded the extent of floor, wall, ceiling and roof damage in four categories: Less than 24 %; Between 25 % and 49 %; Between 50 % and 74 %; and more than 75 %. For approximately 47 % of TGH houses, roof damage was extensive (>75 %), while approximately 35 % of TGH houses suffered extensive wall damage.

Fig. 2 explains the colour tagging criteria of the UNDP survey. The

Table 1
Construction data required at the building/element level for the numerical assessment of a prototype model.

Group Construction Parameter				Survey Range	Prototype Value	Justification
Coomotum	Decilding alon	(i)	Vulnerability ^b	41 m ²⁻ 136 m ^{2,} square or	59 m ² rectangular plan	Median
Geometry	Building plan dims, Footprint	(i)	Em; En; Ot	rectangular	(including porch)	Median
	Building	(i)	He; Ot	1.04–3.17 m elevated height;	2.00 m elevated height;	Average values
	elevation dims	(1)	ric, ot	2.35–2.65 m wall stud height	2.48 m wall stud height	riverage varaes
Roof	Shape	(i)	Em; En; He	Hip	Hip	As surveyed buildings
	Slope	(i)	Ot	18°-33° (Main); 11°-13° (Porch)	21° (Main);	Average values
	•				12° (Porch)	Ü
	Overhang length	(i)	-	0.40-0.71 m	0.51 m	Average
	Frame elements material ^c	(i), (ii), (iii)	Em; He; Ot	Timber	Pitch Pine Timber	(ii) & (iii)
	Frame elements dims	(i)	-	$0.05{-}0.06~m \times 0.10{-}0.15~m$	0.05 m× 0.10 m	As majority
	Frame elements spacing	(i)	En	Jack rafters: 0.61-0.80 m; Main rafters: 0.61-0.87 m	Jack rafters: 0.70 m Main rafters: 0.70 m	Average values, with equal rafter spacing
	Sheathing material ^c	(i)	Em; En	Plywood	Plywood	As surveyed buildings
	Sheathing dims	(i), (ii), (iii), (iv)	-	Unknown	12.7 mm thickness	Minimum requirements
	Cover material ^c	(i)	Em; En; He; Ot	Galvanised sheeting	Galvanised sheeting	As surveyed buildings
	Roof cover dims	(i), (ii), (iii), (iv)	-	Unknown	24-gauge (0.5 mm)	(iv)
Walls	Frame elements material ^c	(i)	Em; En; He; Ot	Timber	Pitch Pine Timber	(ii) & (iii)
	Frame elements	(i)	-	Studs: 0.05-0.08 m	Studs: 0.05×0.10 m; Corner	Majority of wall studs;
	dims			\times 0.05–0.10 m Corner studs:	stud: 0.10×0.10 m; Wall	all corner studs; majority
				0.10×0.10 m; Wall plate:	plate: 0.05×0.10 m; Sill	of wall plates; sill plate
				$0.05{-}0.10$ m \times 0.10 m; Sill plate: 0.05×0.10 m	plate: $0.05 \times 0.10 \text{ m}$	as wall plate
	Frame elements spacing	(i)	En	0.60-1.33 m	0.94 m	Average value
	Cladding material ^c	(i)	Em; En; He	Timber & Sheetrock; Timber & Plywood; Timber	Pitch Pine Timber	(ii) & (iii)
	Cladding dims	(i)	-	0.01-0.04 m thickness	0.02 m thickness	Average value
	Opening	(i)	-	Doors: wood/metal; Windows:	Doors: wood	As majority of surveyed
	material ^c			wood /glass & wood/ PVC/ aluminium	Windows: aluminium & glass	buildings
	Opening dims (%	(i)	Ot	Front elev.: 21 %-26 %; Back	Front elev.: 23 %; Back elev.:	Average values
	of elevation)			elev.: 14 %-15 %; Side elev.:	15 %; Side elev.: 18 % and	
				17 %-27 %	24 %	
	Opening locations	(i)	-	All elevations	All elevations	As surveyed buildings
Floors	Frame elements material ^c	(i)	-	Reinforced Concrete; Timber	Pitch Pine Timber	(ii) & (iii)
	Frame elements dims, Joists	(i)	-	$0.05 - 0.13 \text{ m} \times 0.10 - 0.15 \text{ m}$	Primary Joist: 0.13×0.15 m Sec.ry Joist: 0.10×0.10 m	As surveyed buildings
	Frame elements spacing	(i)	-	0.56-0.61 m	0.61 m	As majority
	Decking material ^c	(i)	En	N/A; Timber	Pitch Pine Timber	(ii) & (iii)
	Decking dims	(i)	-	N/A; 12.7 mm thickness	12.7 mm thickness	As surveyed buildings
Foundations	Type	For external /	Em; En; Ot	Pillars; Strip	Pillars	As majority
	Material	above ground	Ot	Reinforced concrete	Reinforced concrete	As surveyed buildings
	Dimensions	elements: (i)	-	0.23-0.25 m by 0.25-0.43 m	0.26 m by 0.26 m	As surveyed buildings
	Reinforcement	For internal /	-	Unknown	4no. 12.7 mm dia. long. bars,	Long. bars: (iv); conf.
	details	below ground			8d conf. bars at 0.23 m	bars: (ii) & (iii)
		elements: (ii), (iii)		5 1 6 1 11	spacing	
	Layout	& (iv)	<u> </u>	Regular/irregular grid	Regular grid	As majority

Notes:

damage levels relate to the extent of failure observed, rather than damage mechanisms or severity. Therefore, they are insufficient to determine specific vulnerability to wind. The quantitative damage extent is compared to the extent of the failure progression output by the numerical model. Fig. 3 shows the locations of these buildings across the island and their associated damage levels. Fig. 3 also maps the wind speed coordinates obtained from a wind field model for Dominica Hurricane Maria (2017) [18].

Done et al. [18] presented a novel and globally applicable approach to modelling the surface wind field of landfalling tropical cyclones, which capture several aspects of the dynamic and spatial variability of the event and its evolution. The output is a map of the tropical storm's lifetime max. 1-min average wind at a height of 10 m above ground level. For the Hurricane Maria landfall to Dominica, Done's model provided the maximum 1-min sustained wind speed at 1 km grid spacing and they were used with the UNDP damage data to produce cumulative damage curves for typology TGH. Buildings assigned a green tag colour were subdivided assigning 'Damage State 0 to the ones labelled as 'No Damage'.

Fig. 4 shows the damage state exceedance cumulative curves. The building coordinates in the damage assessment are provided to an accuracy of the same order of the size of the building, 10–15 m; therefore,

^a Information obtained by (i) Field survey, or (ii) Local surveyors or (iii) Local engineers or (iv) Local guidelines

^b Empirical (Em), Engineering-based (En), Heuristic (He) or Other (Ot) e.g., data mining fragility and vulnerability methods

 $^{^{\}mathrm{c}}$ In terms of material, this will include information on e.g., wood species, age, and quality if possible

Table 2Construction data required at the level of connections for the numerical assessment of a prototype model.

Group	Construction Parameter	Source of information ^a	Used in Fragility and Vulnerability ^b	Survey Range	Prototype Value	Justification
Roof	Connection types	(i), (ii), (iii), (iv)	Em; En; Ot	Roof cover fastener and purlin to rafter: Screws; Rafter to ridge board: Nails; Rafter to rafter: Nails / Timber Pins; Rafter to wall plate: Nails / Metal Plates / Timber Pins	Roof cover fastener and purlin to rafter: Screws; Rafter to ridge board, rafter to rafter, and rafter to wall plate connections: Nails	As surveyed buildings; rafter to rafter as rafter to ridge board; rafter to wall plate as other roof connections
	Connection materials		En	Steel; Timber	Steel	As majority
	Connection dimensions		En	Unknown	See Table 6 and Table 7	(iii) & (iv)
	Connection spacing		En	Roof cover fastener: 0.12–0.30 m	Roof cover fastener: 0.3 m	Worst-case measurement
Walls	Connection types	(i), (ii), (iii), (iv)	Em; En; Ot	Wall stud to wall plate / sill plate: Screws / Timber Pins; Bracing to corner stud / sill plate: Nails; Wall sheathing: Nails / Slotted panels	Wall stud to wall plate / sill plate, Bracing to corner stud / sill plate, Wall sheathing: Nails	As other connections; as building survey; as majority
	Connection materials		En	Steel; Timber	Steel	As majority
	Connection dimensions		En	Unknown	Table 6 and Table 7; Sill plate to joist: 2no. 10d, 0.15 m long nails, with 0.08 m penetration. Sill plates and joists running parallel are modelled as a single member in SAP2000	(iii) & (iv)
	Connection spacing		En	Wall sheathing: 0.15 m at edge studs, 0.10 m at internal studs	Wall sheathing: 0.15 m at edge studs, 0.10 m at internal studs	(i) & (iv)
Floors	Connection types	(i), (ii), (iii), (iv)	-	Floorboards: Nails; Joist to joist: Nails / Metal Plates / Timber Pins; Joist to foundation: Anchor bolts	Floorboards: Nails; Joist to joist: Nails; Joist to foundation: Anchor bolts	As majority; conservatively as majority
	Connection materials		-	Steel; Timber	Steel	As majority
	Connection dimensions		-	Unknown	Table 6 and Table 7; Joist to foundation: 12.7 mm dia. anchor bolts 0.04 m to 0.05 m deep	(iii) & (iv)
	Connection spacing		-	Floorboards: 2no. nails per board	Floorboards: 2no. nails per board	As majority

Notes:

Table 3
Damage states adopted throughout this study according to the classifications used in the Dominica building damage assessment. After [56,57].

Building Tag Colour	Damage State	Building Damage Level	Description
Green	DS0	No Damage	No damage.
	DS1	Minimal Damage	Roof with less than 25% damage.
Yellow	DS2	Minor Damage	Roof with more than 25% damage.
Orange	DS3	Major Damage	Roof totally damaged as well as
			walls.
Red	DS4	Destroyed	Building completely destroyed. At
			least 50% of walls severely
			damaged.

within the 1 km grid of the wind speed model there is much variability of building typology and local distortions of the wind field which affect the actual damage. This is further heightened by most of the buildings being located near the coast and in the densely populated capital Roseau. By numerically assessing a building typology's structural response to wind loading, the progression through various damage states may be observed in greater detail, and the findings can, in turn, feed back into the exercise of deriving empirical damage functions using cumulative curves.

2.3. Field survey

To address the relative data scarcity on Caribbean residential construction, a detailed field survey was undertaken in Dominica by the

UCL research team. Data collection was completed over 3.5 months in the field to survey 60 residential buildings, covering four typologies, targeting 1–3 storey residential structures tagged with level DS2 and DS3, as per UNDP damage assessment, and exposed to a range of wind speed to minimise sample biases. The success of a survey depended on the consent of the residents.

During the field reconnaissance, the UCL research team visited 310 residential buildings included in the UNDP database, which had not undergone major reconstruction: 117 of these houses were identified as having issues with classification: 17 % of them presented location/coordinate issues, 41 % an incorrect building size, and 63 % the wrong roof shape. This last error is probably due to accessibility/visibility issues on site and/or human error. The most common misclassification of roof types related to hip and valley roofs being recorded as hip roofs, or,

^a Information obtained by (i) Field survey, or (ii) Local surveyors or (iii) Local engineers or (iv) Local guidelines

^b Empirical (Em), Engineering-based (En), Heuristic (He) or Other (Ot) e.g., data mining fragility and vulnerability methods



Green Tag

"Minimal or no damage. Owners or renters do not require assistance to safely live in the building. This often includes damage in windows, doors and small damage in galvanized sheeting."



Orange Tag

"Major repairs are required and often include replacement of rafters and roofing but no wall or structural elements."



Yellow Tag

"Minor repairs required: buildings that require roofs repairs, mainly galvanize sheeting. In principle, rafters do not need to be replaced. However, rafter status must be carefully examined before galvanized sheeting is properly installed."



Red Tag

"Complete rebuilding required: in addition to roofing and rafters, at least 50% of the walls are severely damaged. If repairs are possible, these may be more complex and expensive than a complete rebuilding of the structure."

Fig. 2. UNDP criteria for colour tagging as used in Dominica building damage assessment [56].

more rarely, hip roofs classified as gable roofs. To handle this error hip/hip and valley/cross-hipped roofs were combined when defining building typologies and conducting statistical analyses. However, the misclassification between hip and gable roofs, without knowing the full extent of this error across the entire database, must be noted as a limitation in validating the numerical assessment against the empirical findings.

For the TGH typology, detailed internal and external structural inspections were carried out for four timber frame buildings across the island, whose location is shown in Fig. 3. Geotagged photographs, sketches, building attributes, and structural damage data were collected and collated as part of the fieldwork. The structural details for the three houses built before Hurricane Maria (2017) were used to produce a representative single-storey prototype building with an internal footprint area of $51.1~\text{m}^2$. Table 1 and Table 2 (see Section 2.1) summarise the size range for each of the structural details surveyed, whilst also providing the value adopted for the prototype model and its justification (see Fig. 5).

2.4. Structural model

To assess the wind vulnerability of timber frame buildings, the proposed finite element (FE) model encompasses two stages: 1) an initial test of the robustness of the timber frame and 2) a full assessment of the building, including cladding. Fig. 5 provides plan and elevations of the prototype building, including the configuration of frame elements, the location of openings, and the layout of the interior walls. The building is elevated on reinforced concrete pillars, with anchor bolts connecting the timber frame to the foundations. Table 1 and Table 2 provide the structural details assigned to element and connection of the prototype building. The number, locations, and sizes of openings on external walls of the model are determined to correspond to the average of those surveyed in the field. The building hence is classified as partially open enclosure according to ASCE 7–22.

A 3D frame model is built using SAP2000 [15]. The joist-to-foundation and the joist-to-joist connections are modelled as pinned, in line with the modelling of pinned wall stud-to-wall and sill plate connections by Martin et al. [39]. Timber wall studs are modelled with moment releases in their local 3rd axis only (see Fig. 6), to model the partial rotational restraint imposed by the toe-nailed connections at the wall and sill plates. This differs from Martin et al. [39] approach. The rafter-to-rafter and rafter-to-wall plate connections are modelled as pinned, following Martin et al. [39]. Pfretzschner et al. [43] modelled the roof truss-to-wall connection as rigid; however, it was considered that a toe-nailed connection allows some rotation of the rafter. Shivarudrappa and Nielson [51] modelled a nonlinear rafter-to-wall plate connector; however, in the absence of experimental data, this solution was not adopted. It is assumed that the sill plates are connected to the joists using 2no. 10d, 0.15 m length smooth shank nails, penetrating 0.08 m into the joist while accounting for the thickness of the timber floorboards [33]. For simplicity, the sill plates and joists running parallel are modelled as a single member with equivalent stiffness.

As buildings belonging to this typology were encountered in the field both with and without wall corner bracing elements, this is also incorporated as a sensitivity check. The bracing elements when present, are modelled with moment releases in their local 2nd axis. The sizing of the structural elements for the prototype building are summarised in Table 4 together with the materials' characteristic values used in the analysis.

3. Numerical analysis

3.1. Demand and capacity assessment

Asiz et al. [6] and Pan et al. [41] recorded the wind speed values at which structural failure occurred in numerical FE models of low-rise timber buildings. Asiz et al. [6] consider failure by uplift of the toe-nailed truss-to-wall plate connections, this being the uplift force at a nail exceeding its peak force capacity. Pan et al. [41] considered several

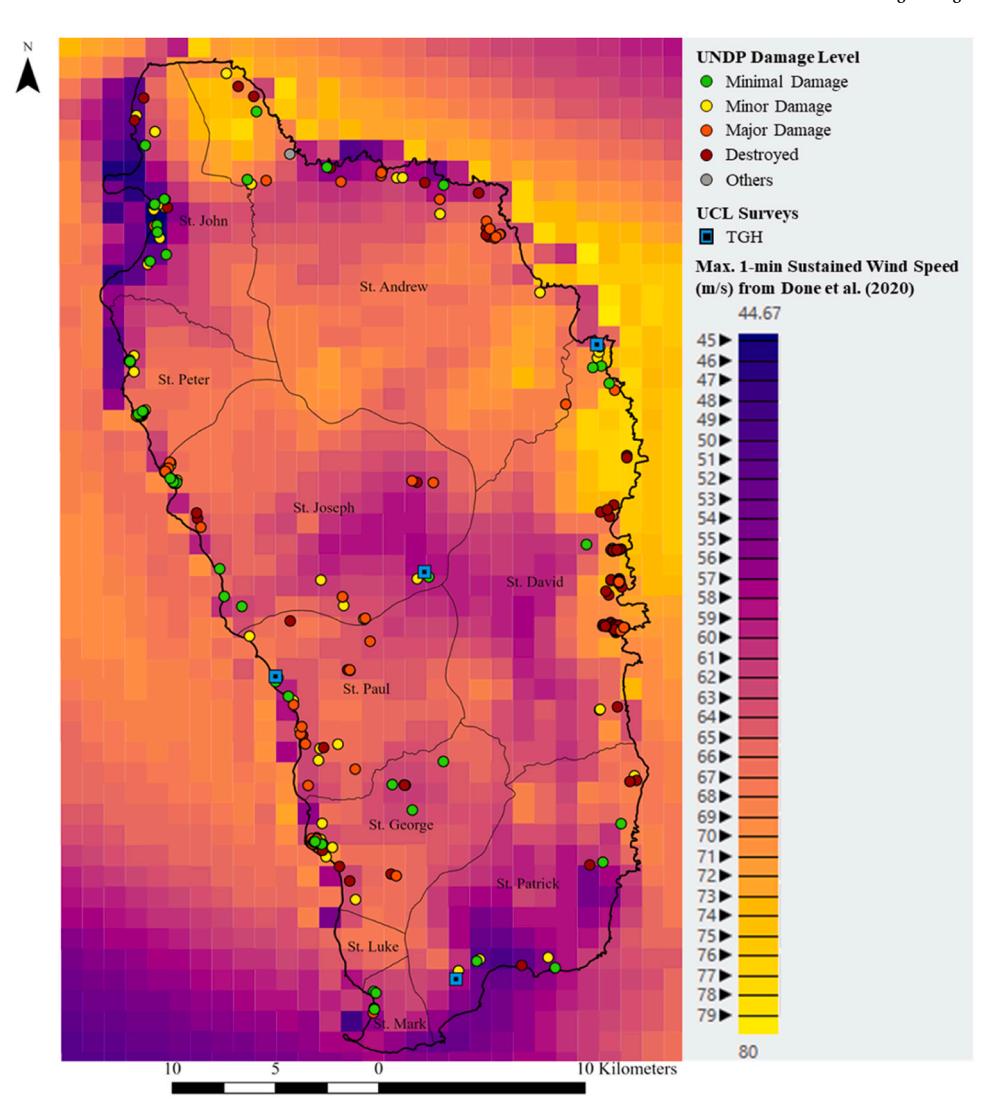


Fig. 3. UCL field survey locations and Dominica Hurricane Maria (2017) Building Damage Map for typology TGH according to UNDP assessment, superimposed with max. 1-min sustained wind speed (m/s) coordinates (1 km by 1 km grid) from UCAR wind field model [18].

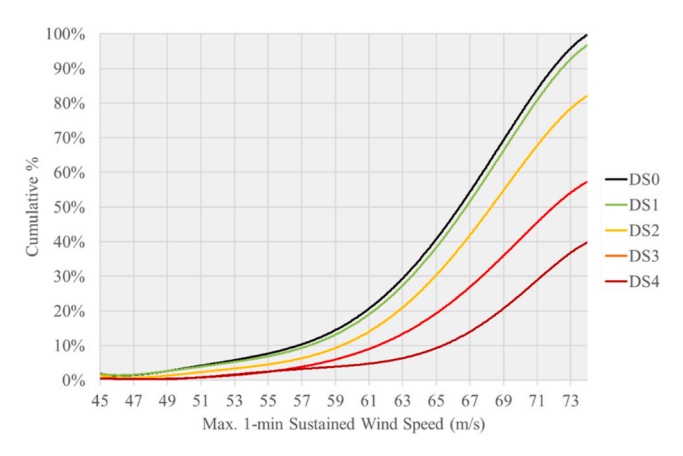


Fig. 4. Cumulative damage grade functions based on the UNDP assessment of 262 residential buildings in typology TGH and UCAR wind field model.

failure mechanisms for various nailed connections, failing when either axial or transverse force in the nails reach their ultimate capacity. This study adopts an incremental ultimate capacity approach to track the progression of structural failures with increasing wind speed values.

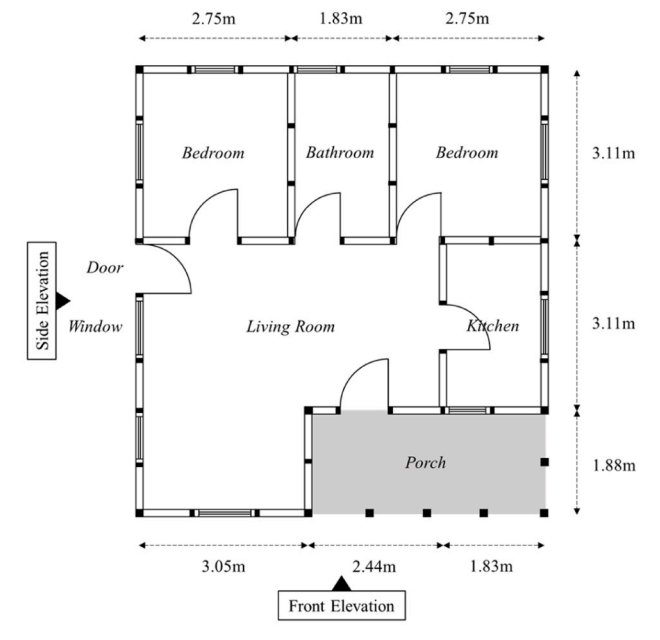
3.1.1. Wind loading

This study reviewed two sources of wind speed data for Hurricane Maria (2017). The wind field model mapped in Fig. 3 [18] shows the maximum 1-min sustained wind speed over land in Dominica to be 76 m/s. Gibbs [24] reports the maximum 3-s gust wind speed at 165mph or 74 m/s. The ASCE 7 Standard adopts the maximum 3-s gust wind speed as an intensity measure. As such, in the FE model, distributed wind forces are applied to the frame elements in increments from zero to 75 m/s, until global failure is attained. The wind loads are calculated and applied to the frame according to ASCE 7–22 Main Wind Force Resisting System (MWFRS) Case 1, with wind approaching perpendicular to the front elevation (see Fig. 7). This is done to analyse the windward roof-to-wall junction with a large overhang over the porch, which is assumed to be the most vulnerable elevation.

The wind pressures for the MWFRS of buildings are determined by the following equation:

$$p = qK_dGC_p - q_iK_d(GC_{pi})$$
(1)

where q and q_i are equal to q_h , the velocity pressure computed at the mean roof height, h_r . K_d is the wind directionality factor, taken as 0.85 for MWFRS Method 1. The gust effect factor, G, is taken as 0.85. The external pressure coefficient, C_p , is determined based on ASCE 7–22 for the roof, walls, and elevated floor. Where required, linear interpolation



(a) Floor Layout

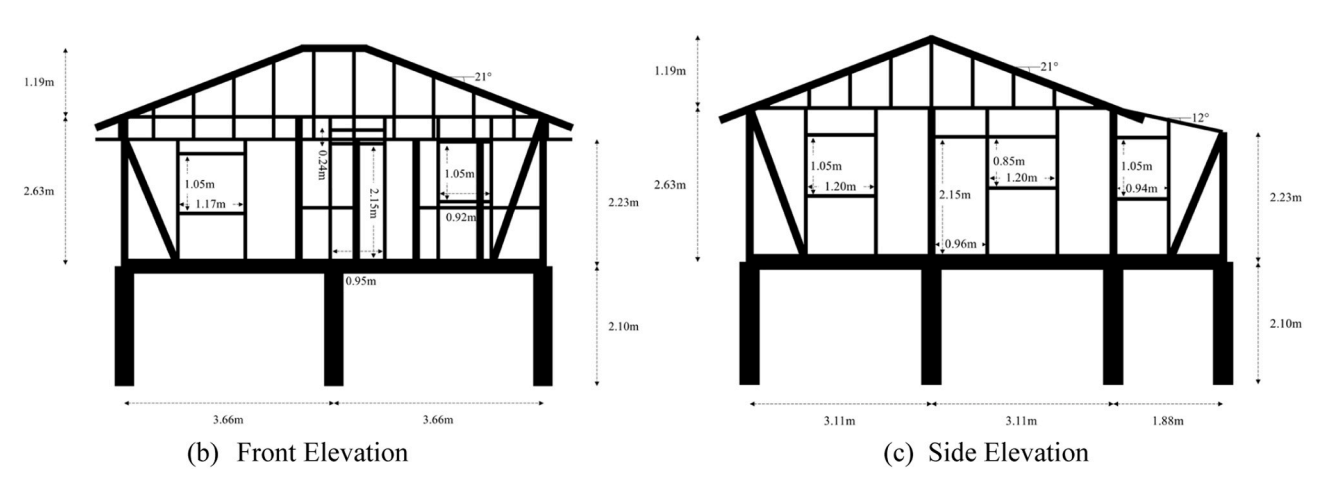


Fig. 5. One-Storey TGH Residential Building Typology.

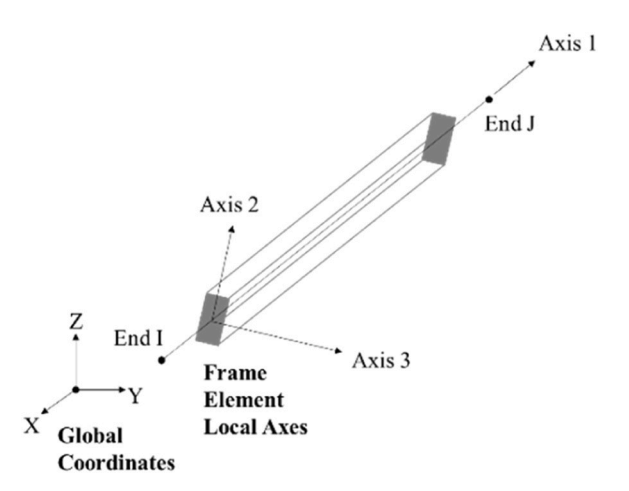


Fig. 6. Global coordinates and frame element local axes as in SAP2000 [15].

is used to determine C_p values based on the building's geometric ratios. Where two values of C_p were listed, the worst-case value was taken, resulting in the largest absolute net pressure values acting on the structural elements once the internal pressures were incorporated. Thus, the external pressures on the windward roof slope are only considered as generating traction. Values for the external pressure coefficients are provided in Table 5. The positive external pressure on the bottom surface of the windward roof overhangs was determined using $C_p = 0.8$ and combined with the top surface pressures determined in Table 5. In the calculation of lateral wind loads acting on the pillars below the elevated building, Eq. (1) is used with $C_{pi} = 0$ and q_h referred to the h_f , height of the floor above the ground. The projected areas of the structural elements perpendicular to the wind direction were taken neglecting shielding, using the C_p values provided for the windward and leeward walls.

Two values, + 0.18 and -0.18, are assumed for the internal pressure coefficient, GC_{pi} under the building's partially open enclosure classification. The velocity pressure q_h (in N/m²) is computed as follows:

$$q_h = 0.613K_zK_{zt}K_eV^2 (2)$$

where K_z is the velocity pressure exposure coefficient at height z. For

Table 4Sizing of structural elements for prototype building typology TGH.

Structural Element	Sizing	Material	Poisson's ratio	Modulus of Elasticity (MPa)	Density (kg/ m ³)
Ridge Board	0.05m×0.10m	Pitch Pine, Isotropic	0.347 [21]	9,900 [21]	747 (10% m.c.) [40]
Rafter (Hip, Main, Jack)	0.05m×0.10m	Pitch Pine, Isotropic	0.347 [21]	9,900 [21]	747 (10% m.c.) [40]
Wall Plate	0.05m×0.10m	Pitch Pine, Isotropic	0.347 [21]	9,900 [21]	747 (10% m.c.) [40]
Wall Stud	0.05m×0.10m	Pitch Pine, Isotropic	0.347 [21]	9,900 [21]	747 (10% m.c.) [40]
Bracing	0.05m×0.10m	Pitch Pine, Isotropic	0.347 [21]	9,900 [21]	747 (10% m.c.)
Corner Stud	0.10m×0.10m	Pitch Pine, Isotropic	0.347 [21]	9,900 [21]	747 (10% m.c.)
Sill Plate	0.05m×0.10m	Pitch Pine, Isotropic	0.347 [21]	9,900 [21]	747 (10% m.c.) [40]
Primary Joist	0.13m×0.15m	Pitch Pine, Isotropic	0.347 [21]	9,900 [21]	747 (10% m.c.)
Secondary Joist	0.10m×0.10m	Pitch Pine, Isotropic	0.347 [21]	9,900 [21]	747 (10% m.c.) [40]
Pillar	0.25m×0.25m	Reinforced Concrete, C16/20	0.2 [9]	28,608 [9]	2,549 [9]

exposure category C, for residential buildings in Dominica, and the height z=h=5.25~m, for the prototype building, K_z is 0.87. The analysis being for a generic prototype, the topographic factor K_{zt} and the ground elevation factor K_e are taken as 1.0, V (in m/s) being the incremental 3 s gust wind speed value. The wind pressures acting on roof, walls and flooring are calculated based on tributary areas and applied as uniformly distributed loads (UDL's) on the frame elements. The effect of overhangs on the wall plate and rafters is captured by the application of an equivalent moment at the rafter to wall plate connection point. All appropriately quantified gravity loads are included in the analysis, in an initial step prior to the application of the wind load with a total value of approximately 220 kN.

In the absence of experimental data, the literature has been reviewed to identify sources quantifying the capacities of the various structural and non-structural connections relevant to this non-engineered timber residential typology. Sections 3.1.2 to 3.1.6 quantify the capacities of nailed and screwed connections and are provided by sources dating from the 1990's as design values. The recent study on timber-concrete bolted connections by Cao et al. [10] provides characteristic capacities. This study is concerned with three types of local failure commonly observed: (1) pull-out failure when a fastener is pulled out from the holding member below due to wind-induced uplift; (2) slip failure, caused by shear action at the joint; and (3) pullover failure, when a member fails/fractures while the connecting fastener is still intact within the holding member. These three local failure modes are schematically illustrated in Fig. 8.

3.1.2. Withdrawal resistance for frame elements

The model is initially assumed to have no damage. Two basic connection failures are explored: pull-out and slip failure of the smooth shank nails, relevant to the connections summarised in Table 6 and represented in Fig. 9, based on the fieldwork findings and engineering insight [33]. The nail withdrawal capacity, for a smooth shank nail driven into the side grain of a timber member, with the nail axis perpendicular to the wood fibres, is determined according to the following equation [2]:

$$W = 1380 \bullet G^{5/2} \bullet D \tag{3}$$

where W is the normal load-duration axial design withdrawal-resistance per unit length of shank penetration in the fastening member. G is the specific gravity of timber, based on oven-dry weight and volume, taken as 0.72 for pitch pine [40]. D is the nail diameter, which is 3.76 mm for 10d nails. The constant which takes a value of 1380 is converted to 9.515 for SI unit consistency.

The National Design Specification for Wood Construction (2018), requires W, to be multiplied by the toe-nail factor $C_m = 0.67$, for toe-nailed connections (prevalent in the typology TGH). This factor allows for the lesser capacity in both withdrawal strength and the lateral strength, of toe-nails going through the end grain of the side members [8]. In the absence of direct experimental data to validate the capacity of these connections, this factor is applied throughout. The withdrawal resistance values, calculated for the connections found in the prototype, are summarised in Table 6. In two locations, the external walls of the building are aligned with secondary joists of a smaller cross-sectional area than the primary joists. In these locations, it is assumed that the secondary joists are nailed to the primary joists using 4no. nails instead of 2no. nails to support this additional weight.

3.1.3. Lateral resistance for frame elements

The Wood Handbook [21] proposes a "Pre-1991" failure equation based on test loads at joint slips of 0.38 mm, corresponding to the approximate proportional limit load for bright common wire nails in lateral resistance driven into the side grain of seasoned wood at 15 % moisture content. The "Pre-1991" approach was replaced by the theoretical yield model based on five percent offset flexural yield stress [21], which adopts the worst-case yield mode based on different combinations of nail bending and timber bearing. As the present study aims at estimating the maximum lateral strength of the nails, hence accounting for full fastener plasticity, the Pre-1991 empirical equation is used:

$$p = K \bullet D^{3/2} \tag{4}$$

where p is the average load at slip initiation, K is a constant equal to 76.45 for pitch pine with a specific gravity of 0.52 based on oven-dry weight and volume at 12 % moisture content; D refers to the nailshank diameter. The Wood Handbook [21] notes that the ultimate load for nails in softwoods may approach 3.5 times the value obtained by Eq. (4), hence this multiplier is used, assuming as slip failure the exit of the nail from the fastened member, obtaining a capacity of 2429 N. For nails driven into unseasoned timber, as is assumed for this study, a factor 0.75 should be applied to Eq. (4). For toe-nailed connections, the lateral resistance values are multiplied by the toe-nail factor, C_{tn} = 0.83. The capacity value obtained for slip failure in this way is compared to the members' shear forces resultants at all connections, except the rafter to wall plate connection, where it is compared to the axial tension in the rafters. Where bracing is present, the bracing members are nailed horizontally or vertically to the corner studs or sill plates respectively, and so the toe-nail factor, C_{tn} = 1.00 applies. The lateral resistance value obtained for the nailed frame-to-frame connections for the bracing elements equals 2926 N. This value is compared to the members' axial tension.

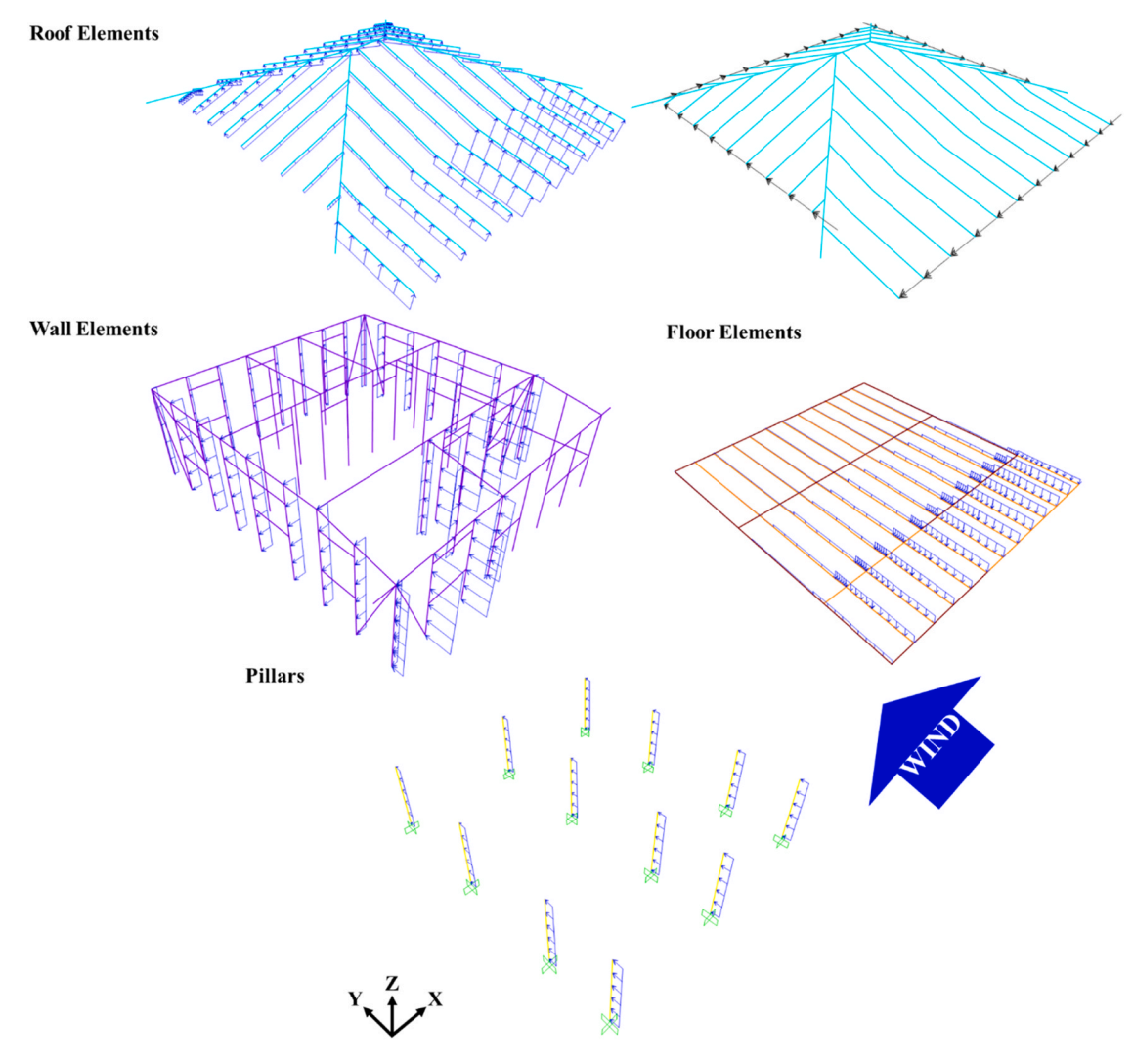


Fig. 7. Wind load UDL's (blue) and moments (black) applied to frame elements in SAP2000 model with bracing, $GC_{pi} = -0.18$ at 56 m/s wind speed according to ASCE 7–22 MWFRS Case 1 with wind approaching perpendicular to the front elevation.

Table 5 External pressure coefficients.

Surface	Geometric Ratio ^{(1),(2),(3)}	C _p ⁽⁴⁾
Windward wall and pillars	All values of L/B	0.8
Leeward wall and pillars	L/B = 1.11	-0.5
Sidewall	All values of L/B	-0.7
Windward 12° roof slope	$h_r/L=0.65$	-0.9
Windward 21° roof slope		-0.4
Leeward 21° roof slope		-0.6
Floor area at 0-0.5h _f distance from windward edge	$h_f/L = 0.27$	-0.9
Floor area at 0.5 h _f -h _f distance from windward edge		-0.9
Floor area at h _f -2h _f distance from windward edge		-0.5
Floor area $> 2 h_{\rm f}$ distance from windward edge		-0.3

Notes:

- $^{(1)}~h_r$ refers to the mean roof height, taken as 5.25 m, whilst h_f refers to the height of the top of the elements below the elevated building, taken as 2.20 m $^{\circ}$
- $^{(2)}$ L refers to the horizontal dimension of the building measured parallel to the wind direction, taken as $8.10~\mathrm{m}$
- $^{(3)}\,$ B refers to the horizontal dimension of the building measured normal to the wind direction, taken as 7.32 m
- (4) Plus and minus signs indicate pressures acting toward and away from the surfaces, respectively

3.1.4. Pullover resistance at pillars

The primary joists are connected to the reinforced concrete pillars using 12.7 mm anchor bolts with a depth of 0.04 m to 0.05 m [33]. The commonly observed failure is pullover due to the vertical loading they carry from the secondary joists in dead, live and wind loading.

The determination of the pullover resistance for bolts is based on the same equation used for screws. The design pullover resistance, $P_{n,over}$, per fastener can be calculated [42] as follows:

$$P_{n,over} = 1.5t_1 d_w F_{u1} \tag{5}$$

where, t_I (in mm) is the thickness of the joist in contact with bolt head; d_w (in mm) is the larger of the diameter of the washer and the bolt head; and F_{uI} (in MPa) is the ultimate tensile strength along the fibres of the member in contact with bolt head or washer. Taking the thickness of the joist as being equivalent to its 0.15 m depth, and the diameter of the washer for a 12.7 mm bolt as 0.03 m [45], the ultimate tensile strength of the pitch pine joists is taken as 2.1 MPa, yielding a pullover resistance of 16,766 N for the joist-to-foundation connection. This is compared to the resultant shear force in the joist.

3.1.5. Lateral resistance at pillars

Cao et al. [10] derived analytical equations to calculate the load-carrying capacity of timber-concrete connections based on the European yield model [12]. For connections without steel pads, the

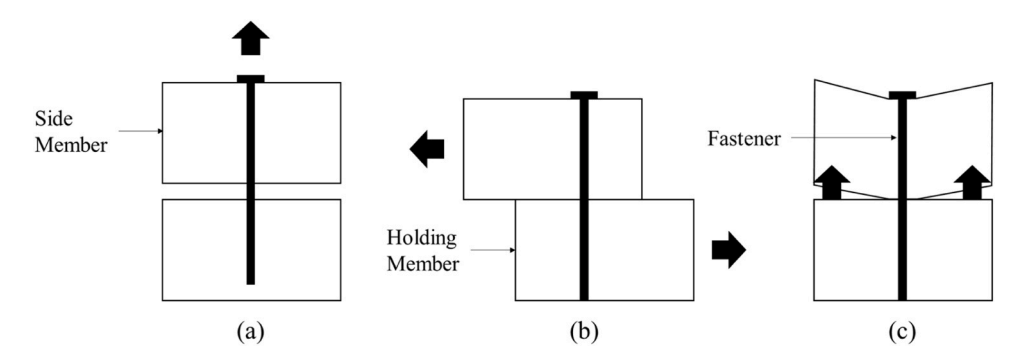


Fig. 8. Schematic illustration of the considered connection failures: (a) pull-out failure; (b)slip failure; and (c) pullover failure.

Table 6Connection withdrawal capacities.

Connection	Description [33]	Nail Diameter (mm)	Penetration Depth (mm)	C_{tn}	Total Withdrawal Resistance for Nails (N)	Force Type
Rafter to ridge board	2no. nails, 0.15 m in length	3.76	101.6	0.67	2143	Axial Tension
Rafter to rafter	2no. nails, 0.15 m in length	3.76	101.6	0.67	2143	Axial Tension
Rafter to wall plate	2no. nails, 0.15 m in length	3.76	63.5	0.67	1339	Shear
Wall stud to wall plate	2no. nails, 0.15 m in length	3.76	101.6	0.67	2143	Axial Tension
Wall stud to sill plate	2no. nails, 0.15 m in length	3.76	101.6	0.67	2143	Axial Tension
Bracing to corner stud	2no. nails, 0.15 m in length	3.76	101.6	1.00	3198	Shear
Bracing to sill plate	2no. nails, 0.15 m in length	3.76	101.6	1.00	3198	Shear
Joist to joist	2no. nails, 0.15 m in length	3.76	101.6	0.67	2143	Axial Tension
Joist to joist (under walls)	4no. nails, 0.15 m in length	3.76	101.6	0.67	4285	Axial Tension

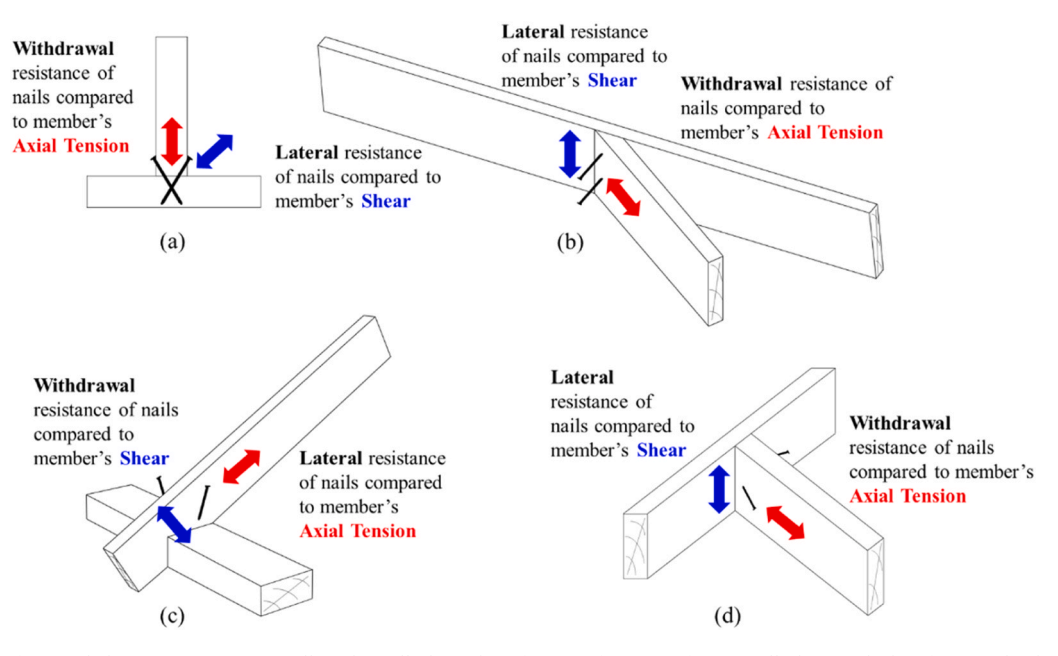


Fig. 9. Illustration of toe-nailed connections at (a) wall stud to sill plate; (b) rafter to rafter; (c) rafter to wall plate; and (d) rafter to ridge board (not to scale).

characteristic load-carrying capacity per shear plane per bolt, $F_{\nu,Rk}$ are computed according to three failure modes which are related to the number of plastic hinges forming in the bolt. For failure mode I, the timber member is crushed without any plastic hinges forming. Mode II involves the formation of one plastic hinge and Mode III two plastic hinges:

$$F_{v,Rk} = \begin{cases} f_{h,k} \bullet d \bullet h, ModeI \\ f_{h,k} \bullet d \bullet h \left(\sqrt{2 + \frac{2d^2 \bullet f_{sy}}{3f_{h,k} \bullet h^2}} - 1 \right), Mode II \\ 2d^2 \sqrt{\frac{f_{sy} \bullet f_{h,k}}{6}}, Mode III \end{cases}$$
(6)

In Eq. (6), $f_{h,k}$ is the characteristic embedment strength, $f_{s,y}$ the yield strength of the bolt, taken at 275 N/mm², d the diameter of the bolt (12.7 mm), and h the thickness of the timber member (0.15 m joists). As noted by Hettiarachchi and Nawagamuwa [31], the characteristic

embedment strength $f_{h,k}$ can be calculated for bolts up to 30 mm in diameter according to the following equation where timber is loaded parallel to the grain:

$$f_{h,k} = 0.082(1 - 0.01d)\rho_k N / mm2$$
 (7)

In which ρ_k refers to the characteristic density of the timber, taken as 747 kg/m³ for pitch pine [40], and d is the diameter of the bolt. As such, the characteristic load-carrying capacity per shear plane per bolt, $F_{\nu,Rk}$ can be calculated and assumed as the lesser from the three failure modes, which occurs for Mode III, at 13,324 N for the joist-to-foundation connection. This is compared to the axial force in the joist in the case of slip failure. At such large resistances, the bolt behaviour is elastic throughout the analysis.

3.1.6. Cladding connections and capacities

The cladding, including timber floorboards, wall sheathing, roof sheathing and metal sheeting of the house are not included in the finite element model; however, their connection capacities are assessed to determine whether they would fail at wind speeds lower than the frame elements. Table 7 summarises the details assumed for the various cladding elements and their connections based on data from fieldwork and the Dominica Housing Guideline recommendations [58]. The 0.05 m by 0.10 m purlins are also not included in the finite element model but are connected by two No.9 wood screws 114.3 mm long [58] to the rafters. The capacity of the nails/screws connecting the cladding, and the purlins are checked for pull-out and pullover failures, using Eq. 3 for the pull-out capacity of nailed connections, and Eq. 5 for pullover resistance for nails and screws, taking $d_{\rm w}$ as the diameter of the nail head.

The design pull-out resistance per screw can be calculated [42] as follows:

$$P_{n,out} = 0.85t_c dF_{u2} \tag{8}$$

with t_c (in mm) the minimum between the depth of penetration (t_n) and the thickness of the member not in contact with the screw head (t_2), d (in mm) the nominal screw diameter and F_{u2} (in MPa) the ultimate tensile strength of the member not in contact with the screw head/washer. When calculating the pullover resistance for screws using Eq. 5, the ultimate tensile strength of the galvanised sheeting is taken as 147 MPa [53]. The withdrawal and pullover resistance values per nail/screw calculated for the various connections are summarised in Table 8. The lesser of the withdrawal or pullover resistances, together with the spacing of the connections is used to calculate a failure UDL to be compared to the UDL applied to the frame elements in the finite element model, in order to determine the wind speed at which the connections of the cladding elements and purlins are expected to fail.

The stiffness of the cladding elements is not accounted for explicitly in the finite element model. Within the assessment a sensitivity check has been conducted, varying the level of constraint that the wall and roof

Table 7 Cladding and associated connection details for the timber residential typology TGH.

Cladding	Connections
24-gauge galvanised sheeting roof cover, 0.5 mm thick [58]	No.9 wood screws, 63.5 mm long according to UNDP [58], spaced at 0.3 m c/c along purlins as worst-case field measurement
12.7 mm roof ply as noted from a survey of a lightweight roof with sheathing	No.9 wood screws, 63.5 mm long at 0.15 m c/c according to UNDP [58]
0.02 m thick tongue and groove timber wall cladding as observed in the field	10d nails according to UNDP [58], 0.15 m spacing at edges, and 0.10 m spacing along inner studs as observed in the field
12.7 mm thick timber floorboards,	2no. 8d nails [58] per board at joists as

observed in the field

0.14 m wide as observed in the field

sheathing can exercise on the frame elements and, hence, alter the structural response.

Four constraint conditions were investigated for the prototype model as follows:

Fully Constrained: translations in the x, y, and z directions were set to be equal across points 1–6 as shown in Fig. 10, representing the extreme case that both the wall and roof sheathing constrain the movement of the structure.

Porch Freed: translations in the x, y, and z directions were set to be equal across points 1–5, whilst point 6 was unrestricted, showcasing the implications of the porch behaving independently from the main structure.

Shear Wall Displacement: translations in the y and z directions were set to be equal across points 1–3. Translations in the x and z directions were set to be equal across points 3–4. Translations in the y and z directions for points 4 and 5 were also set to be equal, whilst point 6 was unrestricted. This allowed for shear wall stiffness, assuming no influence from the roof sheathing.

Free Movement: translations in the x, y, and z directions across points 1–6 were set to be independent, representing the extreme case that both the wall and roof sheathing had no impact on structural movement.

3.2. Failure assessment

The methodology for the failure assessment is summarised in the flowchart in Fig. 11. The linear elastic analysis is first run for applied gravity loads and then for incremental values of wind loads, with an initial wind speed of 20 m/s. The forces are extracted at the joint locations and compared to the connection capacities, as stated in Table 6. If the connection capacities are not exceeded, the analysis moves forward to the next increment in wind loading. If an element's internal forces exceed the connection capacity, the failure is recorded and the corresponding degree of freedom is released. Hip rafters, connected to several other members along their span, can be released at the relevant joint. The analysis is then rerun at the same wind speed value to check for other failures being triggered by the release of the failed element. If no further elements fail, the analysis can continue to the next increment in wind loading. When a frame element is removed from the model, its tributary gravity loads and wind loads are also removed rather than redistributed to the adjacent elements, as the area of cladding associated with the element is also assumed to detach from the structure. This leads to a drop in the recorded base shear. However, this breaching of the building envelope is not simulated by a corresponding change in the net pressures applied to the adjacent frame elements. As shown in Table 11, the percentage area of cladding lost at the roof, walls, and floors by the end of the analysis, never reaches the 80 % opening ratio required by ASCE 7-22 criteria to change the building's enclosure classification from partially open to open, hence the internal pressure coefficient remains constant throughout the analysis.

The analysis terminates and global failure is assumed once enough elements have been removed at the same wind speed value, causing a drop in base shear (V_b) greater or equal to 10 %. This drop in base shear can be observed for both flexible and stiff models, as shown in Fig. 12 under the fully constrained condition. The reference displacement is measured at the structure's highest point, at the ridge board (see Fig. 10), where vertical displacement due to uplift appears more relevant than the horizontal displacement. It is observed that for the braced structures, the elastic vertical displacement is minimal and is followed by significant ultimate displacement following the loss of stiffness due to several gradual releases of rafter-to-ridge connections which do not occur for the unbraced structures. This vertical displacement is smaller when internal pressures are negative. The horizontal elastic displacement appears significant for the non-braced structures.

Table 8 Cladding and purlin connection capacities.

Connection	t _c (mm)	d (mm)	<i>t</i> ₁ (mm)	d _w (mm)	<i>d_n</i> (mm)	t _n (mm)	$P_{n,out}$ (N)	$P_{n,over}$ (N)	Max. UDL (N/m)
Galvanised sheeting to purlins	50.8	4.5	0.5	8.56	N/A	N/A	408	944	2591
Purlins to rafters	63.5	4.5	50.8	8.56	N/A	N/A	510	1370	3239
Roof sheathing to rafters	50.8	4.5	12.7	8.56	N/A	N/A	408	342	2526
Wall sheathing to edge studs	N/A	N/A	20	7.92	3.76	56.2	884	499	7798
Wall sheathing to inner studs	N/A	N/A	20	7.92	3.76	56.2	884	499	4755
Floorboards to joists	N/A	N/A	12.7	7.13	3.33	50.8	707	285	3992

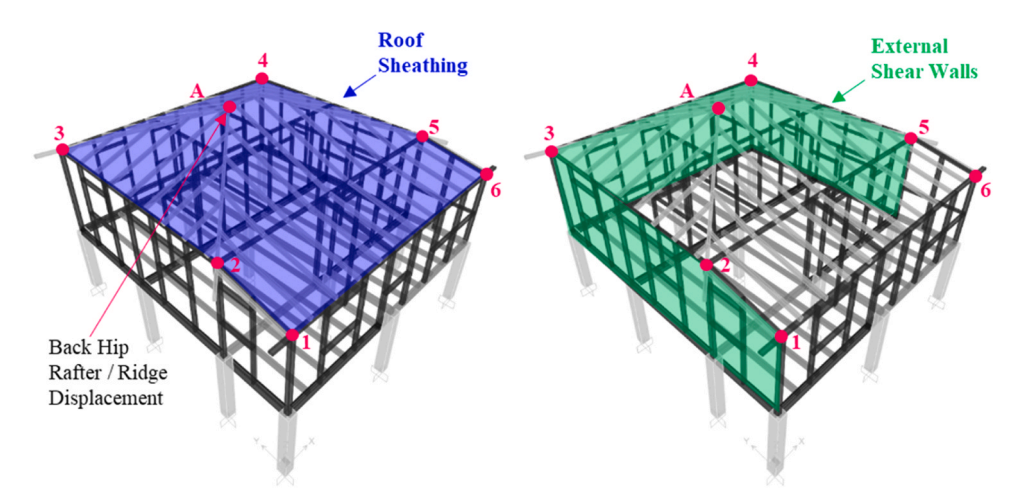


Fig. 10. Joints highlighted at locations where constraints were varied (Points 1-6) and displacements extracted (Point A) from SAP2000.

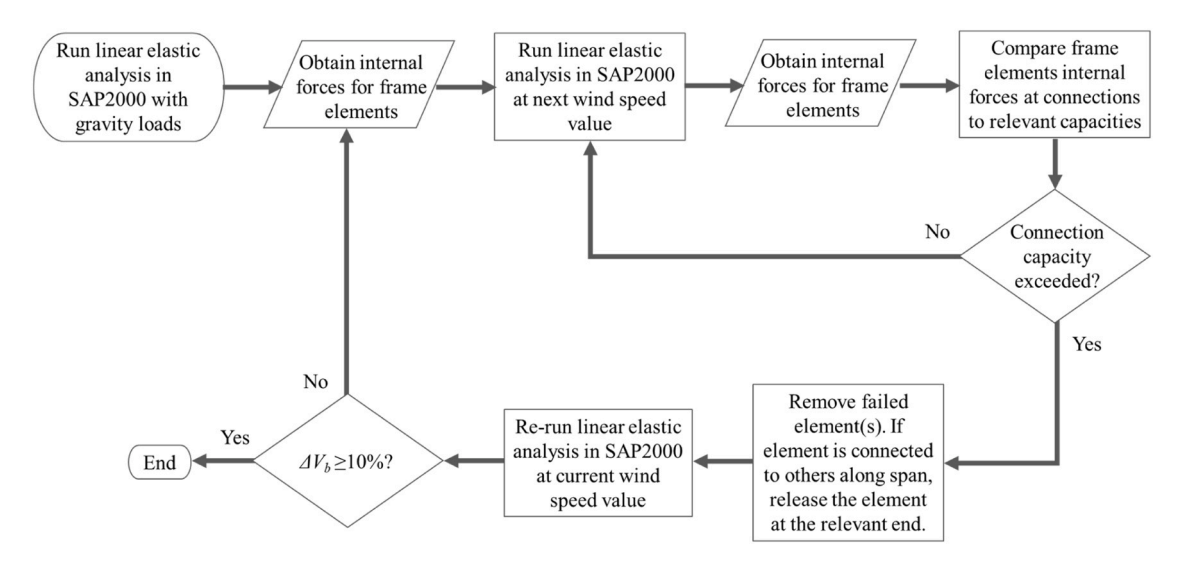


Fig. 11. Flowchart detailing the methodology for the numerical failure assessment.

4. Results

At each increment of wind speed, as loading is applied to the structure, horizontal and vertical displacements are extracted at the location shown in Fig. 10: the highest elevation of the structure, where the ridge board meets a rear hip rafter (A). Fig. 13 shows these displacements against wind speed for the various constraint conditions. The vertical displacement shows initial negative values, due to the gravity loads, before the wind speed increases to cause uplift. Where shear wall displacement or free movement is allowed, and the structure is braced, the horizontal displacement shows initial negative values, due to the asymmetry in the bracing locations, and the shorter bracing elements at the front of the building. The decrease in horizontal or vertical

displacements, as shown by the graphs approaching higher wind speeds, occurs due to the failure and, hence, removal of structural elements within the vicinity of the point at which displacements are being measured. As elements and their associated loading are removed, the displacement at the following step will appear reduced, until a greater increase in wind speed.

Where internal pressures are positive, and the building is not braced, the structural response is quite insensitive to changes in the constraint conditions offered by the roof and wall sheathing. As shown in Table 9, element failures consistently begin occurring at a wind speed of 37 m/s up to 43 m/s when the analysis is terminated. Pull-out of the stud at the re-entrant corner always occurs first, followed by slip failure of the joists at a wind speed of 38 m/s, which is the governing failure mechanism for

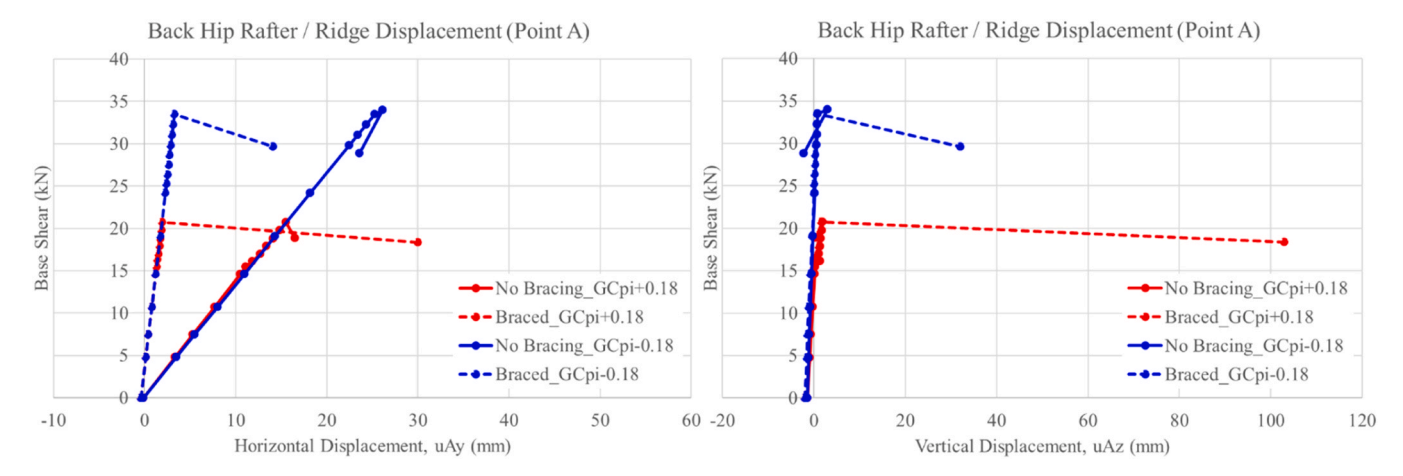


Fig. 12. Base shear vs. horizontal and vertical displacement curves extracted at the Back Hip Rafter / Ridge under the fully constrained condition.

this building under positive internal pressures as shown in Table 11, which details the global failure mechanisms (shown by the failed elements in red) obtained at the final wind speed. Fig. 13 shows that horizontal displacements are generally relatively smaller when the building is slightly more constrained (fully constrained and porch freed cases). As the level of constraint is reduced and free movement is allowed across the six nodes highlighted in Fig. 10, the failure across structural wall elements and the percentage of wall sheathing loss increases. However, the failure across structural roof elements and the percentage of roof sheathing loss is reduced (see Table 10). Table 10 details the number of roof, wall, and floor elements that fail under various bracing, internal pressure, and constraint conditions for the models. In Table 10 the cumulative loss of cladding for the roof, wall, and floor is measured as a percentage of the total area of roof sheathing, wall sheathing, and floor decking respectively.

Where internal pressures are negative, Fig. 13 shows that when the building is slightly more constrained (fully constrained and porch freed cases), the maximum wind speed reached is slightly reduced compared to the unbraced case. In all cases under negative internal pressures where higher wind speeds are reached, Table 10 shows that the number of roof elements failing is greater or equal to the unbraced case. However, under positive internal pressures with lower wind speeds, the number of roof elements failing is reduced in the presence of bracing. Where shear wall displacement or free movement is allowed, but bracing is added, the number of wall elements lost increases. Table 9 also shows that the wind speed at which failure starts to occur reduces in these two cases, as the roof and bracing elements are engaged at earlier stages. Across all constraint conditions, failure of the two front hip rafters is common. In the fully restrained and porch freed cases where the model is braced, a slightly higher wind speed is reached, and the front left hip rafter fails at both ends, leading to significant roof loss. Table 11

Positive internal pressures work in concert with the external pressures applied to the roof and floor elements and the wall frame elements at the back and side elevations. Therefore, element failures are expected to start occurring at lower wind speeds. When the internal pressure is negative, the structure can sustain higher ultimate wind speeds although the failure of the first frame element can occur for similarly low values. For the unbraced structure subject to negative internal pressures, global failure occurs for the highest wind speed, but within a narrow range of them.

Across all constraint conditions, failure of the two front hip rafters is common; however, in the case of positive internal pressures, the back right hip rafter is also engaged and appears to fail consistently. In the majority of cases where bracing is added, Table 9 shows that the wind speed at which failure starts to occur is equal or less, as the roof elements and the bracing elements are engaged at earlier stages. In the case of free movement, failure begins in the studs at the corners of the building,

followed by the bracing, before spreading to the roof. As Fig. 13 shows, after the failure of all bracing elements providing lateral restraint in the y-direction at wind speeds between 43 m/s and 45 m/s, the horizontal stiffness of the building is equal to the unbraced case under both positive and negative internal pressures.

All joists are affected by slip failure, whilst wall studs failed all in pull-out, indicating that they are affected more by the uplift of the roof rather than the lateral pressure. The roof frame elements exhibit pull-out at the rafter-to-rafter or rafter-to-ridge connection and/or slip at the rafter-to-wall plate connection. The failure mechanism shown to recur under positive internal pressures is the slip failure of the joists under the centre of the building, causing a significant breach of the building envelope and hence indicating the vulnerability of elevated structures. Where bracing is present, this failure mechanism is accompanied by either concomitant stud failure or roof failures, depending on the constraint conditions. Under negative internal pressures, many wall studs fail at the front elevation of the building where the porch is located, significantly breaching the building envelope. The bracing elements fail at relatively lower wind speeds and trigger the roof elements' failures. This provides evidence that if the structure is stiffened by bracing, longer and larger nails are required for the frame elements to resist pull-out as more force is attracted to them.

5. Discussion

In the numerical study by Holman et al. [32] on load paths in non-elevated houses with hip roofs and complex geometry, the magnitude of wind uplift forces was found to vary both locally at reactions and globally for net uplift depending on wind direction and the load case applied. Generally, the greatest uplift is concentrated at the corners of the building and around doorways and openings. This agrees with the consistent failure of hip rafter connections (see Table 11) and the pull-out failures of the connections of wall studs and bracing elements at building corners in the present study. Holman et al. [32] also note that the least uplift is under windows and on interior walls that do not have a direct load path from the roof. Regarding the interior walls modelled in this prototype building, where wall stud connections fail in pull-out (see Table 11), this is due to their connection to the floor joists below, to which gravity and wind loads are applied as the building is elevated. For walls which do not extend through the entire building, Holman et al. [32] state that the greatest loads occur for the windward wall. Table 11 shows that where wall stud element connections fail in pull-out, this is consistent for the re-entrant portion of the windward wall.

Fatigue-induced connection failure was not considered in this assessment. As shown by Li et al. [35] high cycle fatigue over a wide range of stress, could cause a reduction in capacity of as much as 41 % of the ultimate. A study by Prevatt et al. [47] found that the ultimate

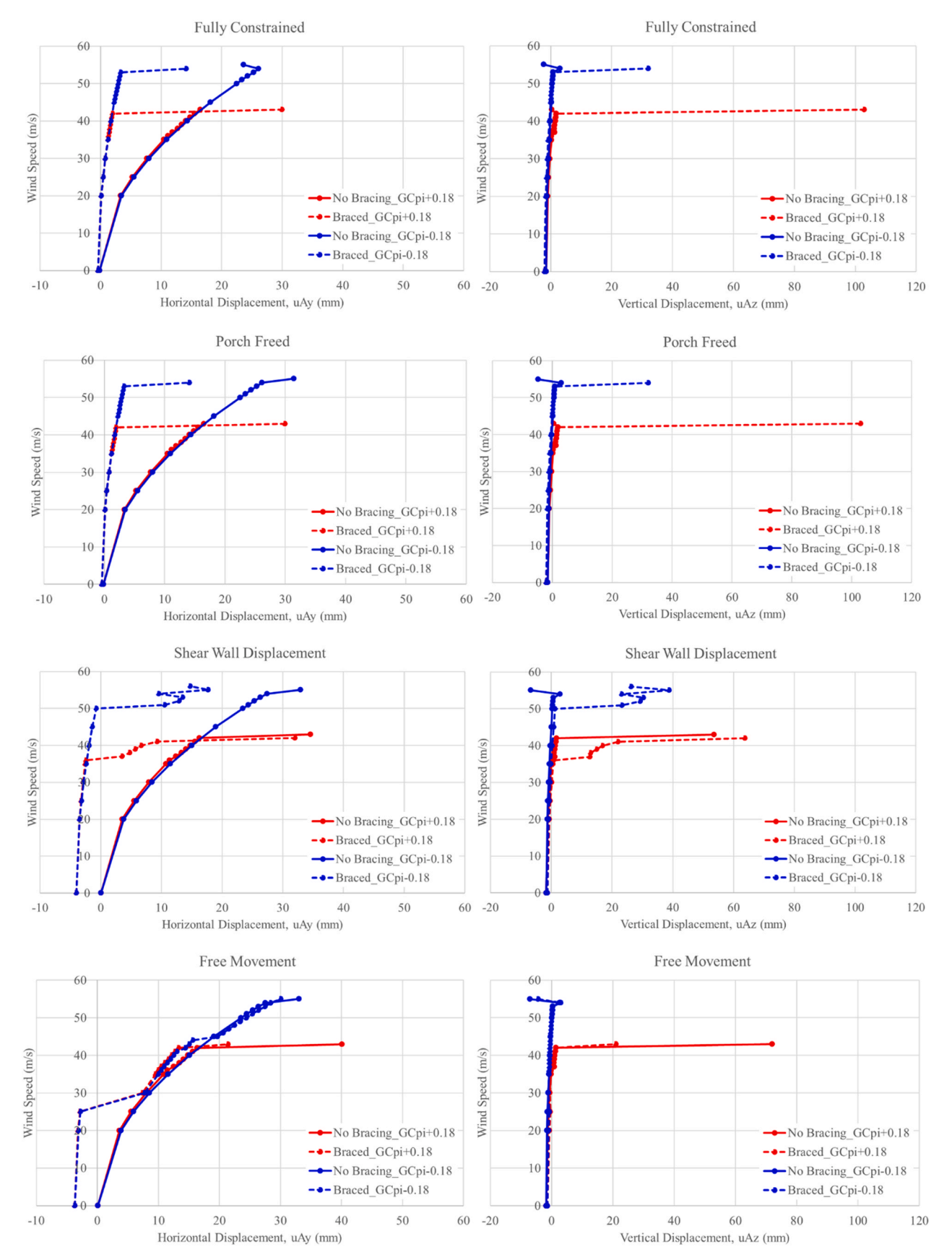


Fig. 13. Wind speed vs. horizontal and vertical displacement curves extracted at the Back Hip Rafter / Ridge under the Fully Constrained, Porch Freed, Shear Wall Displacement, and Free Movement conditions.

Table 9Range of wind speeds for which failure occurs under various internal pressures, bracing and constraint conditions.

Model	Constraint condition								
	Fully Constrained	Porch Freed	Shear Wall Displacement	Free Movement					
No Bracing, $GC_{pi} = +0.18$	37-43 m/s	37-43 m/	37-43 m/s	37-43 m/s					
Braced, $GC_{pi} = +0.18$	38-43 m/s	38-43 m/ s	37-42 m/s	30-43 m/s					
No Bracing, $GC_{pi} = -0.18$	54-55 m/s	54-55 m/ s	54-55 m/s	54-55 m/s					
Braced, $GC_{pi} = -0.18$	54 m/s	54 m/s	51-56 m/s	30-55 m/s					

withdrawal capacity of roof nails in situ (nails driven through wooden sheathing) might be lower than the National Design Specification (NDS) empirically defined values by as much as 33 % [2] for nailed connections exposed to environmental effects and ageing. It is acknowledged that the connections of existing buildings in the field might have lesser capacity than the ones currently assumed in this study using either the NDS [2], the Wood Handbook [21] or Pekoz's [42] equations for the prototype building. While neglecting such effects may overestimate its ultimate performance under hurricane-level wind loading, the proposed approach modelling and assessing individual connections has the capacity to consider degradation effects, and hence improve the results of the numerical model, when data from specific experimental testing of connections and timber species is available.

6. Conclusions

An iterative 3D finite element methodology is developed for the analytical wind vulnerability assessment of low-rise, non-engineered residential buildings. These buildings are considered as highly vulnerable in hurricane events, while adequate data for their detailed structural analysis is difficult to obtain.

The methodology draws on various sources of information, including existing literature, empirical damage data, wind field models, and field survey data, to build and analyse a representative prototype model of a typical residential building typology in the Caribbean, specifically Dominica, where there is a gap in the existing knowledge regarding their construction materials, methods, and structural performance.

The following conclusions are formed based on the discussions of the failure mechanisms of the structural frame of a typical low-rise elevated timber building with a lightweight hip roof under wind loading according to ASCE 7–22 Main Wind Force Resisting System (MWFRS) Case 1, applied to the front elevation. It is noted that this differs from a typical building design, which must consider all wind attack angles from $0^\circ\text{-}360^\circ\text{-}$. The current study is focused on developing a numerical procedure for assessment of structural performance rather than design.

Previous studies that have built full wind analysis numerical models of low-rise timber buildings have been found to exclude elevated buildings and therefore floor and foundation construction details have attracted little attention in wind fragility/vulnerability functions derivation approaches. However, this study's findings show the importance of considering and modelling the floor and foundation construction details for elevated buildings, as the building envelope may be breached through these elements.

The failure mechanisms shown to recur for typology TGH are the slip failure of the joists under the centre of the building under positive internal pressures, and the pull-out of the wall studs at the front elevation of the building near the porch for negative internal pressures. The difference in failure wind speeds between these two conditions is as much as 33 %. The rafter-to-ridge pull-out and rafter-to-wall plate slip failure of the front hip rafter connections appears to be an inherent weakness in the construction of this typology, which eventually leads to the failure of the attached main and jack rafters due to their supporting hip rafter becoming disconnected at both ends. At this stage, the building envelope would be significantly breached at the roof and front elevation, highlighting further the crucial role of the roof frame connections in the building's response to wind loading. The greater observed loss of roof cladding, according to the analysis, occurs for the extreme condition of the full effect of sheathing stiffness for both roof and braced walls for negative internal pressure, up to 27 %. This would represent a loss leading to a damage state DS2 or greater, according to the UNDP damage survey.

Given the distribution of openings on all elevations for the TGH typology, suction forces are most likely to prevail and therefore results associated with negative C_{pi} values are the most realistic, corresponding to values of ultimate wind speed within the range of speeds associated with the Hurricane Maria (2017) wind field model [18].

By assessing the UDLs applied to the frame elements and comparing these values to the capacities of the cladding and purlin connections, computed according to the details contained in the Dominica's Housing Standards (DHS) [58], it is found that these capacities were not exceeded before the frame elements' failures. On the other hand, most of the details of the structural elements adopted for the prototype model, as obtained from the field surveys, fall below the minimum requirements specified by DHS [58]. This includes using nails for frame-to-frame connections rather than metal or hurricane straps (which, for instance in the case of rafter to wall plate connection could increase the capacity by up to 70 %, see Simpson Strong Ties [52]), insufficient rafter and ridge board sizing (0.05mx0.10 m against the prescribed 0.05mx0.20 m), and excessive spacing for wall studs and rafters (700 mm instead of 600 mm).

The inclusion of bracing elements at building corners does not appear to improve the ultimate capacity. The chosen inclination (as observed in the field) is opposite to the one suggested by the DHS, and, has a slightly negative effect on the roof integrity, lowering the wind

Table 10

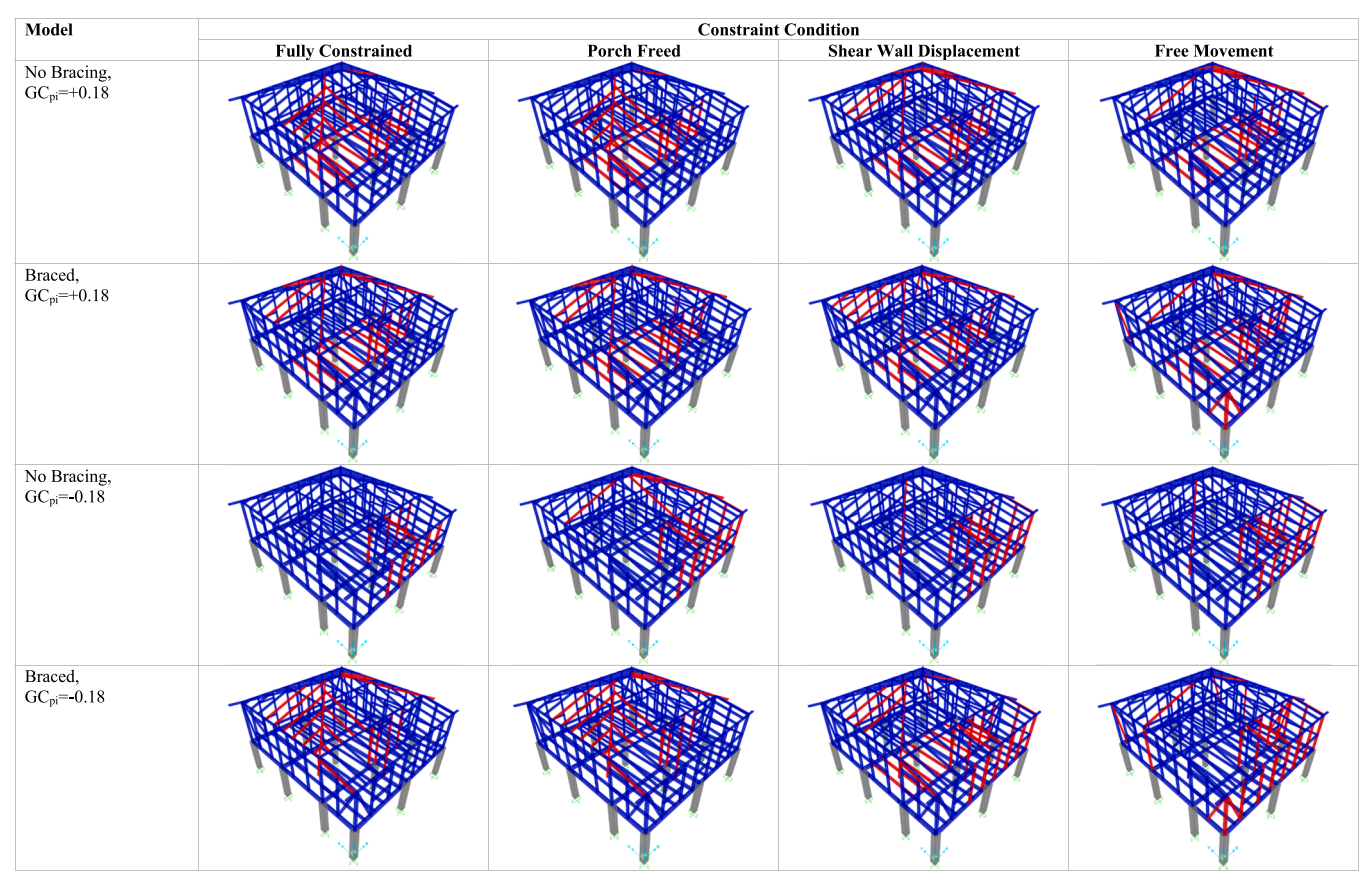
Number of elements (Elm) failed and percentage of cladding (Cld) loss for the roof, wall, and floor under various internal pressures, bracing and constraint conditions.

Model	Losses	s Constraint Condition											
		Fully Constrained		Porch Freed			Shear Wall Displacement			Free Movement			
		Roof	Wall	Floor	Roof	Wall	Floor	Roof	Wall	Floor	Roof	Wall	Floor
No Bracing, GC _{pi} = +0.18	Elm	11no.	6no.	9no.	11no.	6no.	9no.	8no.	6no.	9no.	7no.	7no.	9no.
- *	Cld	18 %	17 %	29 %	18 %	17 %	29 %	15 %	17 %	29 %	15 %	17 %	29 %
Braced, $GC_{pi} = +0.18$	Elm	8no.	7no.	9no.	8no.	7no.	9no.	7no.	8no.	9no.	3no.	13no.	9no.
	Cld	15 %	17 %	29 %	15 %	17 %	29 %	13 %	17 %	29 %	6 %	20 %	29 %
No Bracing,	Elm	1no.	9no.	-	7no.	10no.	-	4no.	12no.	-	4no.	13no.	-
$GC_{pi} = -0.18$	Cld	2 %	17 %	-	16 %	14 %	-	6 %	20 %	-	6 %	23 %	-
Braced,	Elm	15no.	5no.	-	15no.	5no.	-	9no.	13no.	9no.	5no.	23no.	-
$GC_{pi} = -0.18$	Cld	27 %	14 %	-	27 %	14 %	-	20 %	20 %	29 %	13 %	32 %	-

Notes

No. of wall elements include bracing, porch and internal studs which would not contribute to the % of external wall cladding loss

Table 11
Global failure mechanisms at the final wind speed value under various internal pressures, bracing and constraint conditions.



speed at which initial failure occurs.

In the case of negative internal pressures, the onset of structural frame element failures occurs at max. 3-s gust wind speeds between 30m/s-54m/s. Comparing the damage extents detailed in Table 10 to the UNDP damage state definitions in Table 3, it is clear the model can capture conditions corresponding to Damage level DS2 to DS3, identifying portions of roof and wall damage extending to one third of the structure. Terminating the analysis once a 10 % drop in base shear is recorded will mainly reflect the loss of vertical elements in the structure, which no longer transfer the lateral load to the base. This is noted as a limitation in the current failure assessment, and a further measure may be required to determine the termination of the analysis, reflecting the extent of roof and floor element losses.

The validation of the numerical methodology developed by this study arises from the recurring failure mechanisms shown for this building typology modelled under varying conditions. Furthermore, for the model without bracing, experiencing negative internal pressures, the narrow range of wind speeds between the onset of structural damage (54m/s-55m/s) and reaching the final failure mechanism (54 m/s and 56 m/s) also shows agreement with the empirical data assessed for this building typology. It can be noted that 50 % of buildings are at a damage level D1 or above for 67 m/s wind speed. Jiang et al. [34] show that wind flow interference among closely spaced gable-roof buildings, such as those in built-up areas, as opposed to the isolated conditions assumed in the numerical analysis, has a strong effect on critical damaging wind speed. The increase in damaging wind speed can be as much as 14 % from isolated to built-up conditions. These findings correlate well with the difference between the results of the numerical model and the median damaging wind speed determined from the cumulative damage curves of this study (between 16 % and 19 % difference). However, in

this case, the prototype model has a hipped roof. Further studies of grouped building analysis for mixed typologies will shed more light on the correlation between empirical and analytical vulnerability.

This study has shown that the proposed methodology can be effectively used to identify the most fragile assets and prioritise more detailed field data collection and structural assessment procedures for the recommendation of retrofit/reconstruction measures. With data from specific experimental testing of connections and building materials, the proposed approach has the capacity to consider the variability in connection and material properties, etc., and hence improve the results of the numerical model.

CRediT authorship contribution statement

D'Ayala Dina: Writing – review & editing, Validation, Supervision, Project administration, Methodology, Funding acquisition, Conceptualization. **Sarah Esper:** Writing – original draft, Visualization, Validation, Methodology, Formal analysis, Data curation, Conceptualization.

Declaration of Competing Interest

The authors declare that they have no known competing financial interests or personal relationships that could have appeared to influence the work reported in this paper.

Acknowledgements

The work employs field data collected by Sarah Esper with the assistance of Issa Alleyne, Edward Charles, Dailah Felix, Edmund Laville, and Oran Sabaroche. Further information and clarifications required on construction practices, cost, and structural details were obtained through personal communications with Eric James of QSC. Ltd.; Isaac Baptiste of Baptiste & Associates Ltd.; Alistair Grell, Lex Jervier, and Marcus Philbert of SORELL Consulting Ltd. (SCL); Christopher Sorhaindo of ACE Engineering Ltd.; and Jamie Jno Baptiste. The kind participation of the residents of Dominica in this study is greatly appreciated. Funding for this research was provided from the World Bank Group and the EPSRC Centre for Doctoral Training Grant No. EP/N509577/1 and EP/T517793/1.

Data availability

Data will be made available on request.

References

- Alam M, Barbosa A, Mugabo I, Cox D, Park H, Lee D, et al. Elevated light-frame wood residential building physical and numerical modeling of damage due to hurricane overland surge and waves. Eng Struct 2023;294. https://doi.org/ 10.1016/j.engstruct.2023.116774.
- [2] American Wood Council. NDS National Design Specification for Wood Construction: With Commentary. American Wood Council; 2018.
- [3] ANSYS version 12.1. Computer Software. Cecil Township, PA: ANSYS Inc; 2009.
- [4] ASCE. Minimum Design Loads for Buildings and Other Structures ANSI/ASCE 7-02. New York, NY: American Society of Civil Engineers; 2002.
- [5] ASCE. Minimum Design Loads and Associated Criteria for Buildings and Other Structures. American Society of Civil Engineers; 2022.
- [6] Asiz A, Chui YH, Zhou L, Smith I. Three-dimensional numerical model of progressive failure in wood light-frame buildings. World Conf Timber Eng 2010.
- [7] Bertinelli L, Mohan P, Strobl E. Hurricane damage risk assessment in the Caribbean: An analysis using synthetic hurricane events and nightlight imagery. Ecol Econ 2016;124:135–44. https://doi.org/10.1016/j.ecolecon.2016.02.004.
- [8] Breyer D. Design of Wood Structures, Third Edition. New York, NY: McGraw-Hill, Inc: 1993.
- [9] British Standards Institution. 2004. Eurocode 2: Design of concrete structures Part 1-1: General rules and rules for buildings. BS EN 1992-1-1:2004, BSI, London, UK.
- [10] Cao J, Xiong H, Peng T. Load-carrying capacity analysis for timber-concrete bolted connections considering the effect of steel pads. Eng Struct 2021;247:113095.
- [11] CAPRA. 2011. Metodología de Modelación Probabilística de Riesgos Naturales: Vulnerabilidad de Edificaciones e Infraestructura. In Technical Rep. ERN-CAPRA-T1-5.
- [12] CEN 1995 (2004) EN 1995-1-1:2004+A1:2008+A2:2014: Design of timber structures. Part 1–1: General-Common rules and rules for buildings. European committee for standardization, Brussels, Belgium.
- [13] Chock GYK. Modeling of hurricane damage for Hawaii residential construction. J Wind Eng Ind Aerodyn 2005;93(8):603–22. https://doi.org/10.1016/j. iwaia 2005.06.001
- [14] CIMNE (Centro Internacional de Métodos Numéricos en Ingeniería). 2013. Probabilistic modeling of natural risks at the global level: global risk model. Background Paper prepared for the 2013 Global Assessment Report on Disaster Risk Reduction.
- [15] CSI. Structural Analysis Program SAP2000-NonLinear version 19. Computers and Structures, Inc.; 2016 (CSI).
- [16] D'Ayala DF, Tsai PH. Seismic vulnerability of historic Dieh–Dou timber structures in Taiwan. Eng Struct 2008;30(8):2101–13.
- [17] Ding Z, Zhang W, Hughes W, Zhu D. A modified sub-assembly approach for hurricane induced wind-surge-wave vulnerability assessment of low-rise wood buildings in coastal communities. Journal of Wind Engineering and Industrial Aerodynamics 2021;218:104755.
- [18] Done JM, Ge M, Holland GJ, Dima-West I, Phibbs S, Saville GR, et al. Modelling global tropical cyclone wind footprints. Nat Hazards Earth Syst Sci 2020;20(2): 567–80.
- [19] Emanuel K. Global warming effects on U.S. hurricane damage. Weather, Clim, Soc 2011;3(4):261–8. https://doi.org/10.1175/WCAS-D-11-00007.1.
- [20] FEMA Federal Emergency Management Agency. Building Performance: Hurricane Andrew in Florida - Observations, Recommendations, and Technical Guidance. USA: Federal Insurance Administration; 1992.
- [21] Forest Products Laboratory (US), 1999. Wood handbook: wood as an engineering material. The Laboratory.
- [22] Fusco G, Zhu J. Personalized vulnerability assessment of customized low-rise wood-frame residential structures under hurricane wind loads: A flexible scenariobased simulation approach. ASCE-ASME Journal of Risk and Uncertainty in Engineering Systems, Part A: Civil Engineering 2023;9(3):04023023.
- [23] Garcia Palencia AJ, Saffar A, Godoy LA. Fragiligty curves for metal industrial buildings under wind. Rev Int De Desastres Nat, Accid e Infraestruct Civ 2008;8(2): 165–82.
- [24] Gibbs T. Wind Speeds Sel Isl Hurric Irma Maria 2017 2017. (http://www.unc.edu/ims/luettich/jbikman/01_23_2013/Literature%20dump/StatisticalModelsOfHollandPressureProfileParameter.pdf).
- [25] Government of the Bahamas. 2003. Bahamas Building Code, 3rd edition. Available at: https://www.bahamas.gov.bs/wps/wcm/connect/d7ebcbad-f9b6-42e3-aff2-

- 79f83bd91810/Bahamas%2BBuilding%2BCode%2B3rd%2BEd\.pdf? MOD\:\text{AJPERES.}
- [26] Government of the Commonwealth of Dominica 2024. Dominica Housing Recovery Project. Accessed January 21, 2024, from (https://hrp.gov.dm/).
- [27] He J, Pan F, Cai CS. A review of wood-frame low-rise building performance study under hurricane winds. Eng Struct 2017;141:512–29. https://doi.org/10.1016/j. engstruct.2017.03.036.
- [28] He J, Pan F, Cai CS. 'Modeling wind load paths and sharing in a wood-frame building'. Wind Struct 2019;29(3):177–94. https://doi.org/10.12989/ was.2019.29.3.177.
- [29] He J, Pan F, Cai CS, Chowdhury A, et al. 'Progressive failure analysis of low-rise timber buildings under extreme wind events using a DAD approach'. J Wind Eng Ind Aerodyn 2018;182(July):101–14. https://doi.org/10.1016/j. iweja.2018.09.018.
- [30] He J, Pan F, Cai CS, Habte F, et al. 'Finite-element modeling framework for predicting realistic responses of light-frame low-rise buildings under wind loads'. Eng Struct 2018;164(January):53–69. https://doi.org/10.1016/j. engstruct.2018.01.034.
- [31] Hettiarachchi MTP, Nawagamuwa AD. Embedment strength of tropical timber species. Engineer: Journal of the Institution of Engineers. Eng J Inst Eng Sri Lanka 2005;38:1.
- [32] Holman J, Gupta R, Miller TH. Load paths in light-frame wood house with complex geometry. J Archit Eng 2021;27(2):06021001. https://doi.org/10.1061/(asce) ae.1943-5568.0000461.
- [33] Jervier, L. 2022. Email to Sarah Esper.
- [34] Jiang M, Ma H, Wang S, Chen B. Wind-induced fragility of a group of three gableroof buildings with different roof slope and building spacing. Eng Struct 2023;292: 2023. https://doi.org/10.1016/j.engstruct.2023.116532.
- [35] Li L, Gong M, Smith I, Li D. Exploratory study on fatigue behaviour of laterally loaded, nailed timber joints, based on a dissipated energy criterion. Holzforschung 2012;66(7):863–9.
- [36] López HD, Godoy LA. A methodology to estimate structural damage in industrial buildings due to hurricanes. Rev Int Desastres Nat, Accid e Infraestruct Civ 2005;5 (2):121–34.
- [37] López R.R., Godoy L.A., Acosta F.J., Guevara J.O., Lluch J.F., Cruzado J.A.M., 2005. Estimating natural hazards damage for the insurance industry in Puerto Rico. Third LACCEI International Latin American and Caribbean Conference for Engineering and Technology (LACCEI'2005) "Advances in Engineering and Technology: A Global Perspective," June..
- [38] Malone BP, Miller TH, Gupta R. Gravity and wind load path analysis of a light-frame and a traditional timber frame building. J Archit Eng 2014;20(4):1–10. https://doi.org/10.1061/(asce)ae.1943-5568.0000136.
- [39] Martin KG, Gupta R, Prevatt DO, Datin PL, van de Lindt JW. Modeling system effects and structural load paths in a wood-framed structure. J Archit Eng 2011;17 (4):134–43. https://doi.org/10.1061/(asce)ae.1943-5568.0000045.
- [40] MatWeb, (n.d.). The online materials information resource. Available at: (https://matweb.com/search/DataSheet.aspx?MatGUID= 0ab23b5aa55143b8afe30 8793188eb60&ckck=1) (Accessed: 29 June 2023).
- [41] Pan F, Cai CS, Zhang W, Kong B. Refined damage prediction of low-rise building envelope under high wind load. Wind Struct 2014;18(6):669–91.
- [42] Pekoz, T., 1990. Design of cold-formed steel screw connections.
- [43] Pfretzschner KS, Gupta R, Miller TH. Practical modeling for wind load paths in a realistic light-frame wood house. J Perform Constr Facil 2014;28(3):430–9. https://doi.org/10.1061/(asce)cf.1943-5509.0000448.
- [44] Pinelli J-P, Simiu E, Gurley K, Subramanian C, Zhang L, Cope A, et al. Hurric Damage Predict Model Resid Struct 2004. https://doi.org/10.1061/(ASCE)0733-9445(2004)130.
- [45] Portland bolt 2020. Standard Washers. Available at: (https://www.portlandbolt.com/products/washers/standard-flat/) (Accessed: 29 June 2023).
- [46] Prevatt DO, Dupigny-Giroux LA, Masters FJ. Engineering perspectives on reducing hurricane damage to housing in CARICOM Caribbean islands. Nat Hazards Rev 2010;11(4):140–50. https://doi.org/10.1061/(ASCE)NH.1527-6996.0000017.
- [47] Prevatt DO, Shreyans S, Kerr A, Gurley KR. In situ nail withdrawal strengths in wood roof structures. J Struct Eng 2014;140(5):04014008.
- [48] Quinn N, D'Ayala D, Descamps T. Structural characterization and numerical modelling of historic Quincha walls. Int J Archit Herit 2016;10(2-3):300–31.
- [49] Rittlemeyer BM, Roueche DB. Probabilistic wind uplift resistance framework for the relative evaluation of wood-frame load paths. Eng Struct 2024;298. https:// doi.org/10.1016/j.engstruct.2023.116984.
- [50] Sealy KS, Strobl E. A hurricane loss risk assessment of coastal properties in the caribbean: evidence from the Bahamas. Ocean Coast Manag 2017;149:42–51. https://doi.org/10.1016/j.ocecoaman.2017.09.013.
- [51] Shivarudrappa R, Nielson BG. Sensitivity of load distribution in light-framed wood roof systems due to typical modeling parameters. J Perform Constr Facil 2013;27 (3):222–34.
- [52] Simpson Strong Tie 2024)=. Hurricane Ties technical datasheet (viewed 20/10/2024) (https://strongtie.co.nz/sites/default/files/technical_data/Technical% 20Dat%20Sheet_H.pdf).
- [53] Song B, Galasso C, Garciano L. Wind-uplift fragility analysis of roof sheathing for cultural heritage assets in the Philippines. Int J Disaster Risk Reduct 2020;51: 101752
- [54] Sparks P.R., Baker J., Belville J., Perry D.C. 1985. Hurricane Elena Gulf Coast August 29-Sept 2 Committee on Natural Disasters..
- [55] Trautner CA, Ojdrovic RP. Comparison of directional and envelope wind load provisions of ASCE 7. J Struct Eng 2014;140(4):04013100.

- [56] United Nations Development Program (UNDP), 2017. 'BUILDING DAMAGE ASSESSMENT Dominica – Hurricane Maria. Preliminary Findings'.
- [57] UNDP, 2018a. 'Hurricanes Irma and Maria: One year on'.
- [58] UNDP, 2018b. Guide to Dominica's Housing Standards.
- [59] Valdivieso D, Goldwyn B, Liel AB, Javernick-Will A, Lopez-Garcia D, Guindos P. Potential for mitigating hurricane wind impact on informally-constructed homes in Puerto Rico under current and future climate scenarios. Int J Disaster Risk Reduct 2024;110. https://doi.org/10.1016/j.ijdrr.2024.104627.
- [60] Yamin LE, Hurtado AI, Barbat AH, Cardona OD. Seismic and wind vulnerability assessment for the GAR-13 global risk assessment. Int J Disaster Risk Reduct 2014; 10(PB):452-60. https://doi.org/10.1016/j.ijdrr.2014.05.007.
- [61] Yoo Y, Koliou M, Yazdani N. Assessing elevated home slab retrofitting method for residential coastal buildings under hurricane loads. Journal of Building Engineering 2024;86:108994.
- [62] Zisis I.Structural monitoring and wind tunnel studies of a low wooden building. Concordia University.2006.
- [63] Zisis I, Stathopoulos T. Wind load transfer mechanisms on a low wood building using full-scale load data. J Wind Eng Ind Aerodyn 2012;104–106:65–75. https://doi.org/10.1016/j.jweia.2012.04.003.